# CD8 Binding of MHC-Peptide Complexes in *cis* or *trans* Regulates CD8 $^{+}$ T-cell Responses

**Yang Liu [1,†], Michel A. Cuendet [1,2,3,†], Laurence Goffin [1], Radek Šachl [4], Marek Cebecauer [4], Luca Cariolato [1], Philippe Guillaume [1], Patrick Reichenbach [1], Melita Irving [1], George Coukos [1] and Immanuel F. Luescher [1]**

***1 - Ludwig Institute for Cancer Research,*** *University of Lausanne, and Department of Oncology, University Hospital of Lausanne, 1009, Lausanne, Switzerland*

***2 - Swiss Institute of Bioinformatics,*** *1015 Lausanne, Switzerland*

***3 - Department of Physiology and Biophysics,*** *Weill Cornell Medicine, New York, USA*

***4 - Department of Biophysical Chemistry,*** *J. Heyrovsky Institute of Physical Chemistry of the Czech Academy of Sciences, 18223 Prague, Czech Republic*

***Correspondence to Immanuel F. Luescher:*** *Chemin des Boveresses 155, 1066 Epalinges − CH, Switzerland. Fax: +41 21 692 5995. immanuel.luescher@unil.ch*

https://doi.org/10.1016/j.jmb.2019.10.019

***Edited by Ichio Shimada***

## Abstract

The coreceptor CD8αβ can greatly promote activation of T cells by strengthening T-cell receptor (TCR) binding to cognate peptide-MHC complexes (pMHC) on antigen presenting cells and by bringing p56$^{Lck}$ to TCR/CD3. Here, we demonstrate that CD8 can also bind to pMHC on the T cell (in *cis*) and that this inhibits their activation. Using molecular modeling, fluorescence resonance energy transfer experiments on living cells, biochemical and mutational analysis, we show that CD8 binding to pMHC in *cis* involves a different docking mode and is regulated by posttranslational modifications including a membrane-distal interchain disulfide bond and negatively charged O-linked glycans near positively charged sequences on the CD8β stalk. These modifications distort the stalk, thus favoring CD8 binding to pMHC in *cis*. Differential binding of CD8 to pMHC in *cis* or *trans* is a means to regulate CD8$^{+}$ T-cell responses and provides new translational opportunities.



## Introduction

Heterodimeric CD8αβ functions as a coreceptor and can greatly increase the sensitivity and breadth of antigen recognition by CD8$^{+}$ peripheral T cells bearing the T-cell receptor αβ (TCR) [1,2]. The cytoplasmic tail of CD8α carries two vicinal cysteines that bind p56$^{Lck}$ (Lck, lymphocyte-specific protein tyrosine kinase) via a coordinate complex [3]. The basic cytoplasmic domain of CD8β promotes association with lipid microdomains (rafts) and Lck [4, 5)]. By binding to major histocompatibility complex (MHC) class I-peptide complexes (pMHC) associated with the TCR, CD8 strengthens binding to cognate pMHC and brings Lck to the TCR/CD3 complex, thus facilitating Lck-mediated phosphorylation of CD3 immunoreceptor tyrosine-based activation motifs [6−8]. In addition, CD8 can bind to noncognate pMHC in the absence of TCR, which is referred to as accessory function and promotes T cell adhesion and activation [8]. During T cell development, CD8 activity is regulated by changes in glycosylation and sialylation of conserved threonines in the distal CD8β stalk [9−11]. Similar changes occur on T-cell differentiation and activation [12−14]. It has been proposed that these changes modulate the CD8 binding affinity for pMHC, which remains controversial [9,15].

The structures of the CD8α and β stalks are assumed to be extended and semirigid, capable of spanning across the TCR and pMHC variable domain to allow the CD8 Ig domain to bind to the

MHC constant domain [15–17]. Both CD8 stalks contain a membrane proximal and a distal cysteine [9]. Formation of a membrane proximal interchain disulfide bond is important for CD8 chain assembly and intracellular transport [18]. It is not known whether there exists a second interchain disulfide bond, which is not evident because the CD8α and β stalks are asymmetric in terms of length and spacing of their two cysteines.

The X-ray structures of CD8αα and CD8αβ immunoglobulin (Ig) domain in complex with pMHC are similar [17,19]. In the murine CD8αβ-$D^d$ complex, CD8β is positioned near the pMHC α1 variable domain, which allows binding to cognate pMHC on the target cell in spite of its shorter stalk. Before the structure of CD8αβ-pMHC complex was known, mutational analyses were performed to identify the CD8αβ-pMHC docking orientation [20–23]. Several of that data cannot be explained by the known CD8αβ-$D^d$ structure, arguing that there exists a second docking mode. It has been shown that CD8αβ can bind to pMHC on the same T cell (in *cis*), which may involve a different binding orientation, similar to Ly49s that can bind pMHC in *cis* and *trans* using different binding modes [24–29]. It is noteworthy that activated $CD8^+$ T cells express abundant misfolded MHC class I heavy chains that have been reported to interact with different molecules, including CD8, which may involve phosphorylation of its cytoplasmic domain [30].

In the present study, we examined whether the CD8αβ heterodimer can bind pMHC in a different configuration. We used CD8-transduced T cell hybridomas and primary murine T cells, mutational and functional analysis, fluorescence resonance energy transfer (FRET) and in silico modeling to demonstrate the existence of a second CD8αβ-pMHC docking orientation. We show that CD8-pMHC binding on the T cell, in *cis*, attenuates CD8 function and $CD8^+$ T-cell responses, and is regulated by posttranslational modifications, i.e., the presence/absence of a membrane distal interchain disulfide bond and negatively charged O-linked sugars on the CD8β stalk. The biological significance of this new regulatory principle is discussed.

## Results

The stalks of CD8α and CD8β each comprise two cysteines, one of which is membrane proximal and the other distal (Fig. 1A–C). The stalk of CD8β is shorter than that of CD8α, as is the distances between its two cysteines. This implies that if CD8 binds to a TCR-associated pMHC of another cell, the CD8β Ig domain is proximal to the MHC variable domain [17]. Conversely, if CD8 binds to pMHC on the same cell [24,25], it conceivably adopts a reversed orientation, in which the CD8β Ig domain is proximal to the MHC constant domain.

### Modeling and validation of a reversed CD8-pMHC binding orientation

Given the possibility that CD8αβ can bind to pMHC on the same T cell (in *cis*) and the inability of the existing crystal structure of CD8αβ-$D^d$ (in *trans*) to explain all experimental data, notably the effects of several point mutations (Table 1), we explored whether there exists a second docking mode for the CD8 Ig domain on the MHC. To begin, we modeled the CD8αβ-$K^b$ complex starting from random orientations and performing protein-protein docking using the HADDOCK software [31,32]. Ambiguous distance restraints (satisfied if any subset of interatomic distances between two molecular regions is low) were applied to approximately define the target interface regions, without imposing restrictions on the CD8 binding orientation. We obtained two main clusters of energetically stable configurations (Fig. 1D and E). One cluster showed a configuration very similar to the CD8αβ-$D^d$ X-ray structure (Fig. 1F and G) [17]. Strikingly, we also obtained a slightly better scoring cluster, in which CD8αβ is rotated approximately 180° relative to $K^b$ and CD8α proximal to the $K^b$ variable domains (reversed orientation) (Fig. 1H and I). This model showed contacts between the CD8α residues R8, E27, N83 and K84 and the $K^b$ α2 residues E102, R111, Q115 and E128 and (Fig. 1I). To test these predictions, we mutated the $K^b$ residues pairwise and combined, produced biotinylated $K^b$-peptide complexes using the NP356-364 peptide from the lymphocytic choriomeningitis virus (LCMV), and immobilized these on plates. The CD8-mediated adhesion of activated cytotoxic T lymphocytes (CTL) was reduced by about 25% by the $K^b$ E102A/R111A double mutation, slightly more (28%) by the $K^b$ Q115A/E128A double mutation and about 37% by the quadruple mutation (Fig. 1J and K). Because none of these contacts exist in the CD8αβ-$D^d$ X-ray structure [17], these results suggest that CD8-pMHC binding can occur also in an alternate, reversed binding orientation. Qualitatively similar results were obtained when the same docking procedures were applied to CD8αβ and $D^d$ (Fig. S1).

To test this, we took advantage of the known structures of Fab fragments of the anti-CD8α mAb YTS105 and the anti-CD8β mAb YTS156 in complex with CD8 [33,34] and modeled both Fab in complex with our two CD8αβ-$K^b$ models (Fig. S2A and B). This unequivocally showed that the YTS105 Fab could bind unimpeded only when CD8αβ is in a coreceptor-like orientation, and conversely that YTS156 Fab could bind only when CD8αβ is in the reversed orientation (Fig. 1G and H) [17,34]. We then examined whether the YTS105 and YTS156

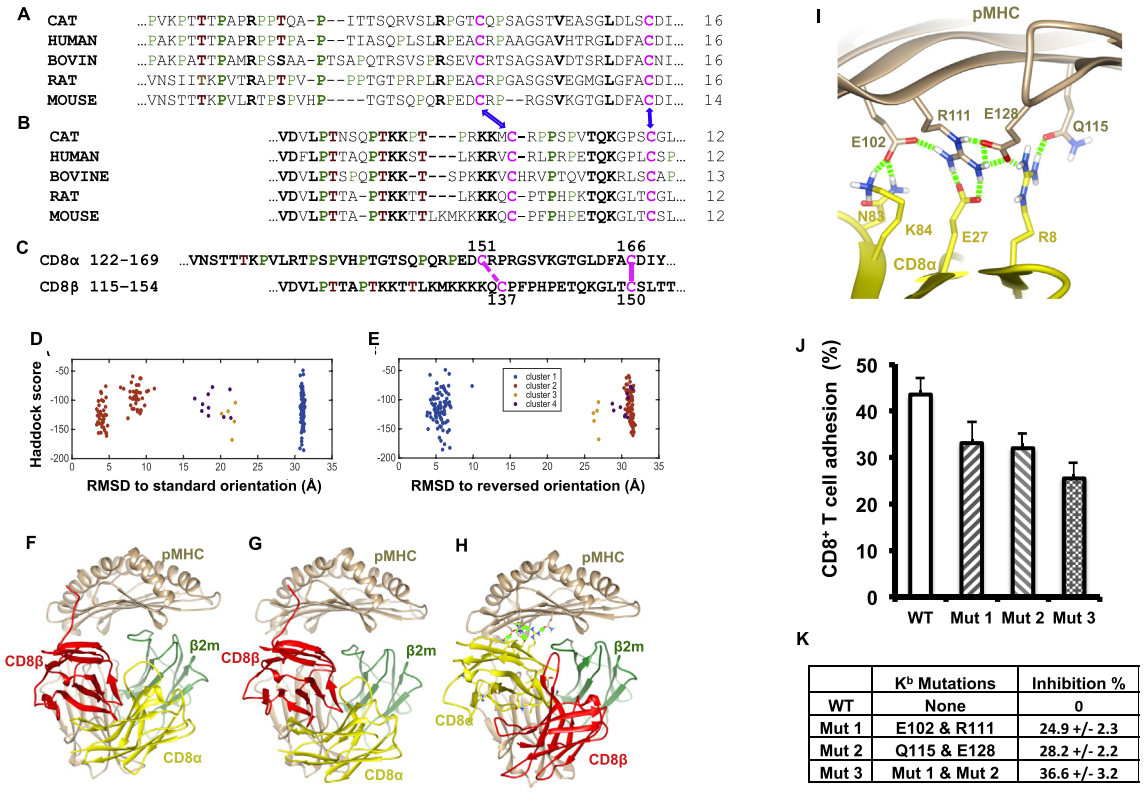


| | $K^b$ Mutations | Inhibition % |
|---|---|---|
| WT | None | 0 |
| Mut 1 | E102 & R111 | 24.9 +/- 2.3 |
| Mut 2 | Q115 & E128 | 28.2 +/- 2.2 |
| Mut 3 | Mut 1 & Mut 2 | 36.6 +/- 3.2 |

**Fig. 1. CD8 stalk sequences and modeling of a novel CD8αβ-pMHC binding mode. (A, B)** The CD8α (A) and CD8β (B) stalk sequences of different species are listed with conserved residues in bold, cysteines in magenta, prolines in green, and threonines in brown. The numbers indicate the residues between the two cysteines. The numbers indicate the amino acids between the two cysteines. **(C)** Amino acid sequences of the stalk regions of mouse $CD8\alpha_{122\text{-}169}$ and $CD8\beta_{115\text{-}154}$, spanning 48 and 40 residues, respectively. Color-coding as in A. The numbers indicate the cysteines. **(D–G)** In silico CD8αβ docking to $K^b$ yielded 200 configurations whose Haddock scores (more negative = better) are plotted as function of the root mean square deviation (RMSD) of CD8αβ backbone atoms calculated on alignment of the MHC α3 domains, relative to the X-ray structure of the CD8αβ-$D^d$ complex (PDB: 3DMM) (D) or the complex in the reversed orientation obtained by superimposing CD8αβ onto CD8αα in complex with $K^b$ (PDB: 1BQH) (E). The configurations represented in cluster 1 (blue) are distant from the orientation of the X-ray structure (3DMM), but close to the initial reversed orientation. The configurations represented in cluster 2 (red) show slightly lower scores and are similar to the coreceptor orientation (3DMM). **(F)** Structure of mouse CD8αβ in complex with $D^d$ (PDB; 3DMM). **G.** Docking model of the CD8αβ-$K^b$ complex in coreceptor orientation. Ribbons in tan indicate $D^d$ or $K^b$, green β2m, red CD8β and yellow CD8α. **(H, I)** Docking model of the CD8αβ-$K^b$ complex in reversed orientation (H). The predicted hydrogen bonds between residues of CD8α (yellow) and the $K^b$ variable domains (in tan) are shown as green dashed lines (I). **(J, K)** Activated $CD8^+$ splenic T cells were labeled with crystal violet and incubated with anti-CD3 mAb 145.2C11 in 96-well plates coated with $K^b$ LCMV $NP_{205–212}$ complexes. After washing, the percentage of adhered T cells was determined via the crystal violet absorbance (J). Mean values and SD were calculated from two experiments (K).

Fab inhibit cytokine responses. To this end, activated P14 $TCR^+$ T cells bearing $CD8\alpha\beta_{WT}$ were incubated with $D^b$ transduced P815 cells, preloaded with the LCMV GP33 peptide variant KAVYNLATM in the absence or presence of the Fab fragments. Consistent with our modeling, YTS 156 Fab strongly inhibited the IFNγ and TNFα responses, whereas the YTS 105 did not (Fig. S2C and D). It is noteworthy that YTS 156 Fab avidly inhibited both cytokine responses already at low concentrations, whereas YTS 105 Fab was inhibitory only at high concentrations. These results pointed toward the existence of "reversed" orientation of CD8αβ available to bind with anti-CD8β, resulting in inhibition of T cell activation. Similar findings were obtained in a previous study, which also pointed out steric constraints of YTS 105 antibody binding to T cell–associated CD8-pMHC complexes [34]. It is noteworthy that the anti-CD8α mAb 53.6.72 binds to an epitope similar as the one recognized by mAb YTS 105 and inhibits CD8-mediated adhesion, but not cognate pMHC binding (Fig. S2E) [8,33–35]. This is consistent with our finding that mutations targeting the reversed orientation had a strong impact on CD8-mediated adhesion (Fig. 1I–K).

Table I. CD8αβ binding to pMHC in *cis* or *trans* involves different contacts [19–21,23,64–66].

| Reversed Orientation | | | Coreceptor Orientation | | Comments and mutational analysis | | |
|---|---|---|---|---|---|---|---|
| Model: $K^b$-CD8αβ[1] Structures: | | | $D^b$-CD8αβ[2] | $K^b$-CD8αα[3] | | | |
| $K^b$ | CD8α | $D^d$ / $K^b$ | CD8α | CD8α1 | Assay/mutation | Effect[4] | References |
| E102 | N83 | E102 | No contact | No contact | | | |
| R111 | E27 | R111 | No contact | CD8α1 | IL-2 production/E27A | -2 | 19, 21 |
| Q115 | R8 | Q115 | No contact | No contact | Tetramer binding/R8A | -3 | 23 |
| E128 | R8 | E128 | No contact | No contact | Tetramer binding/R8A | -3 | 23 |
| D212 | S58, N82 | D212 | No contact | No contact | | | |
| T214 | S59, Q34 | T214 | No contact | CD8α1 | | | 19 |
| T216 | Q34 | T216 | No contact | CD8α1 | | | 19 |
| Q226 | S108 | Q226 | S37 | CD8α1 | Esterase release/Q226A | -2 | 19, 64 |
| D227 | No contact | E227 | Y55; H60 | No contact | | | |
| M228 | S108 | M228 | No contact | CD8α1 | IL-2 production/M228A | -3 | 65 |
| E232 | S31 | E232 | No contact | CD8α1 | Tetramer binding/S31A | -1 | 23 |
| | | | | | | | |
| $K^b$ | CD8β | $D^d$ / $K^b$ | CD8β | CD8α1 | Assay/mutation | | References |
| E222 | S101 | E222 | No contact | CD8α2 | IL-2 production/S101A | -1 | 19-21, 23 |
| E223 | G100 | E223 | No contact | CD8α2 | $^{51}$Cr release/E223K | -1 | 19, 66 |
| I225 | Y32 | I225 | S101 | No contact | | | |
| Q226 | Y32 | Q226 | P102 | CD8α2 | Esterase release/Q226A | | 19, 65, 66 |
| D227 | S30, S53, S54 | D227 | No contact | CD8α2 | IL-2 production/S53A;S54A | -2 | 19, 20, 66 |
| E229 | K55 | E229 | No contact | No contact | IL-2 production/K55A | -3 | 20, 21, 66 |

1 The $K^b$-CD8αβ model in reversed orientation is shown in Figs. 1J,K
2 The $D^d$-CD8αβ X-ray structure is shown in Fig. 1H and documented in PDB 3DMM
3. The $K^b$-CD8αα X-ray structure documented in PDB 1BQH. CD8α1 is proximal to the $K^b$ variable domain
4. The inhibitory effect of the mutations increases from -1 to -3

## Mutation of CD8β cysteine C137 and C150 has opposing effects on CD8 Ig domain membrane proximity and T cell function

The existence of two alternate binding configurations of CD8αβ requires structural elements conferring flexibility, namely in the CD8 stalks. Indeed, the CD8αβ–pMHC *cis* binding mode requires a kink in the CD8 stalk to bring the CD8 Ig domain closer to the plasma membrane of the same T cell. We examined whether interchain disulfide bonds in the CD8 stalks could favor such a kink. The stalks of CD8α and CD8β each comprise two cysteines, one of which is membrane proximal and the other one distal, a feature that is highly conserved among mammalian species (Fig. 1A–C).

To understand the contribution of each cysteine to the assembly and configuration of CD8αβ, we mutated the CD8β stalk cysteines in position 137 or 150 to serine, and introduced wild type (WT) $CD8\beta_{WT}$, $CD8\beta_{C150S}$ or $CD8\beta_{C137S}$ into T1.4 T cell hybridomas, which express the T1 TCR and wild type CD8α, but not CD8β [4,5] (Fig. S3). The CD8α expression in the mutant CD8β transfectants was slightly lower compared with the hybridomas expressing $CD8\beta_{WT}$ or CD8α only. The CD8β expression in the $CD8\beta_{C150S}$ mutant was lower compared with the $CD8\beta_{C137S}$ mutant, possibly because of impaired intracellular transport [18]. To gauge the distance of the CD8αβ Ig domain to the plasma membrane, we used FRET measurements based on fluorescence lifetime imaging microscopy (FLIM). Living T cell hybridomas were stained with Alexa 488 labeled Fab fragments of the anti-CD8β mAb 53.5.81 (donor) and the membrane dye 1,1′-dioctadecyl-3,3,3′,3′-tetramethylindodicarbocyanine 4-chlorobenzenesulfonate (DiD) (acceptor). The average FRET efficiency measured on hybridomas expressing $CD8\alpha\beta_{WT}$ was substantially lower than on those expressing $CD8\alpha\beta_{C150S}$, but higher than on hybridomas expressing $CD8\alpha\beta_{C137S}$ (Fig. 2A,C,D). Because $CD8\alpha\beta_{C150S}$ has solely the membrane distal interchain disulfide bond (between $CD8\alpha_{C151}$ and $CD8\beta_{C137}$) and $CD8\alpha\beta_{C137S}$ has the membrane proximal one (between $CD8\alpha_{C166}$ and $CD8\beta_{C150}$), these results indicate that the former disulfide bond favors CD8 immunoglobulin domain membrane proximity, whereas the latter disfavors it. When the cells were washed with acidic buffer, to dissociate cell surface pMHC complexes [26,27], a substantial reduction in FRET efficiencies was observed, especially on cells expressing $CD8\alpha\beta_{C150S}$ (Fig. 2B). This argues that the interchain disulfide bond between

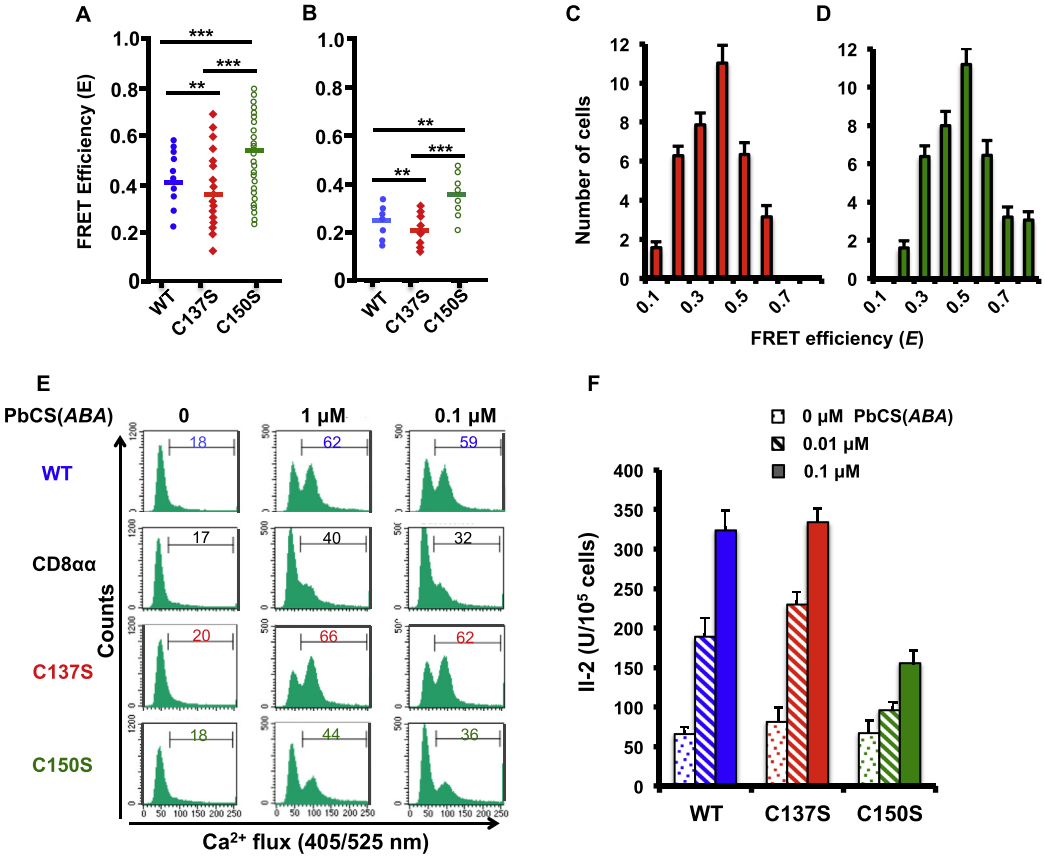


**Fig. 2. Mutation of the CD8β stalk cysteine 137 and 150 differently affect the CD8 Ig domain orientation and T1 T cell hybridoma function. (A)** T1.4 hybridomas expressing CD8αβ wild type ($_{WT}$) (blue) CD8α$\beta_{C137S}$ (red) or CD8α$\beta_{C150S}$ (green) were labeled with Alexa 488 conjugated Fab fragments of the anti-CD8β mAb 53.5.8 and with lipophilic 1,1′-dioctadecyl-3,3,3′,3′-tetramethylindodicarbocyanine, 4-chlorobenzenesulfonate (DiD). The average proximity between the CD8β Ig domain and the plasma membrane was measured as a change in the fluorescence lifetime of the donor (Alexa 488) in the presence of the membrane acceptor (DiD). Each dot represents the FRET efficiency (*E*) of a cell and the bold horizontal bars their mean values. **(B)** The experiment was repeated after removal of their surface pMHC complexes by acid wash. **(C, D)** Histograms represent the number of cells in the indicated FRET efficiency ranges measured on T1.4 hybridomas expressing CD8α$\beta_{C137S}$ (C) or CD8α$_{C150S}$ (D). Mean values and SD were calculated from the data shown in A. **(E)** T1.4 T cell hybridomas expressing CD8αβ, CD8αα, CD8α$\beta_{C137S}$ or CD8α$\beta_{C150S}$ were labeled with Indo-1 and incubated with P815 cells (ratio = 1/1) previously pulsed with graded concentrations of PbCS(*ABA*) peptide. After 5 min intracellular $Ca^{2+}$ mobilization was measured by flow cytometry as a ratio of the Indo-1 fluorescence emissions at 405 and 525 nm. **(F)** Alternatively, the hybridomas were incubated with P815 cells previously incubated with 0 (open bars), 0.01 µM (doted bars) or 0.1 µM (full bars) PbCS(*ABA*) peptide and after 16 h the IL-2 of the supernatants was measured by ELISA. Mean values and SD were calculated from three experiments.

CD8α$_{C151}$ and CD8β$_{C137}$ favors a conformation of the CD8 stalk that increases CD8 Ig domain membrane proximity, whereas the membrane proximal interchain disulfide bond does not.

The above data suggest that expression of the two CD8β stalk mutations affect CD8 function. To test this, we asked whether T cell hybridomas expressing the CD8β$_{WT}$ or mutant CD8β chains would display different functionality. T1 T cell hybridomas expressing CD8αα, CD8αβ$_{WT}$, CD8αβ$_{C150S}$ or CD8αβ$_{C137S}$ were assayed for response to P815 cells pulsed with 1 µM PbCS(*ABA*) peptide, by measuring intracellular $Ca^{2+}$ flux. Compared with CD8αβ$_{WT}$ cells, the CD8aβ$_{C150S}$ mutation impeded intracellular $Ca^{2+}$ flux to nearly the same low level as observed for CD8αα expressing cells (Fig. 2E). By contrast the CD8αβ$_{C137S}$ mutation slightly increased intracellular $Ca^{2+}$ levels. These differences were more striking at lower antigen concentration (0.1 µM PbCS(*ABA*) peptide). Similar findings were obtained when antigen-induced IL-2 release was assessed (Fig. 2F). This increase is explained by that the CD8β$_{C137S}$, mutation decreases the CD8 Ig domain membrane proximity i.e., allows a fully extended configuration, in which CD8 is best reactive as coreceptor (Fig. 2A–D) [17].

We next extended these investigations to primary T cells, on which CD8 is subject to activation/differentiation dependent posttranslational modification [12,14,15]. First we assessed the CD8 Ig domain membrane proximity on activated primary T cells expressing CD8$\alpha\beta_{WT}$, CD8$\alpha\beta_{C137S}$ or CD8$\alpha\beta_{C150S}$ by means of donor fluorescence reduction. To this end the cells were stained with Alexa 488 labeled anti-CD8β 53.5.81 Fab fragment alone or together with octadecyl-rhodamine B (R18), which being lipophilic, binds to the plasma membrane and absorbs the Alexa 488 fluorescence in a distance-dependent manner [26]. The R18-mediated reduction of Alexa 488 fluorescence intensity (MFI) was larger on CD8$\alpha\beta_{C150S}$ (73.6%) than on CD8$\alpha\beta C_{137S}$ expressing cells (61.1%) (Fig. 3A and B), indicating that the CD8 Ig domain of CD8$\alpha\beta_{C150S}$ was closer to the membrane than that of CD8$\alpha\beta_{C137S}$.

To assess the function of activated primary T cells, we transduced splenic T cells from P14-TCR transgenic CD8β knockout (KO) mice with CD8α plus CD8$\beta_{WT}$, CD8$\alpha\beta_{C150S}$ or CD8$\alpha\beta_{C137S}$. Similar to the hybridoma, CD8α expression in transfectants with mutant CD8β was slightly lower compared with the hybridomas expressing wild type CD8β or CD8α only (Fig. S4). We assessed the IFNγ response of these cells on incubation with $D^b$ transfected P815 cells (P815/$D^b$) pulsed with the LCMV 33–41 peptide variant KAVYNLATM. As assessed by intracellular cytokine staining, the IFNγ response of cells expressing the CD8$\beta_{C150S}$ mutant was markedly reduced relative to cells expressing CD8$\alpha\beta_{WT}$ (nearly threefold lower number of IFNγ$^+$ cells), while those expressing CD8$\alpha\beta_{C137S}$ showed about 20% more IFNγ$^+$ cells than wild type (Fig. 3C). Similar differences were observed at different peptide concentrations, or when TNFα responses were assayed (Fig. 3D). In addition, the CD8$\beta_{C150S}$ mutation resulted in marked loss of the cytotoxic response, as assessed by CD107a surface

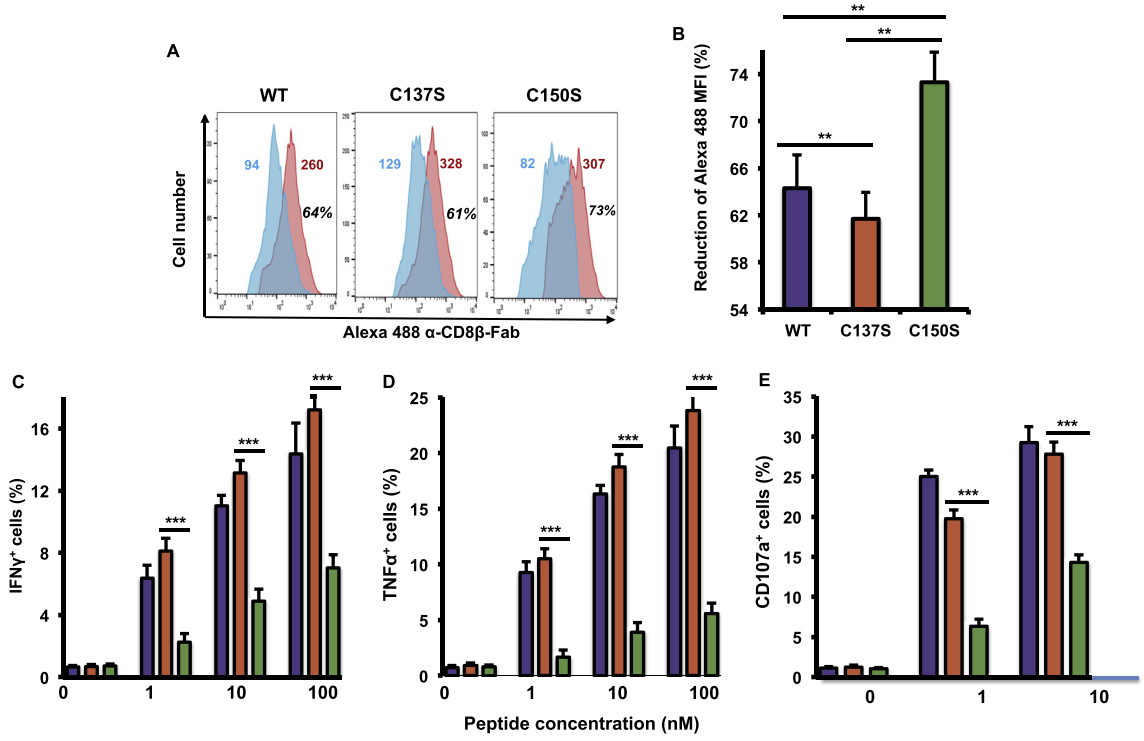


**Fig. 3. Mutation of the CD8β stalk cysteine 137 and 150 differently affect the CD8 Ig domain membrane proximity and responses of primary CD8$^+$ T cells. (A)** Splenocytes from CD8β KO, P14 TCR transgenic mice were transduced with CD8α cistronically linked to CD8β wild type. After 8d the CD8$^+$ T cells were stained with Alexa-488 labeled α-CD8β-Fab fragment (red histograms) or costained with octadecyl rhodamine B (R18) (blue histograms). The blue and red numbers indicate the corresponding Alexa-488 MFI and the black ones the reduction of the Alexa 488 fluorescence caused by R18, calculated as 100 × [$MFI_{Alexa\ 488\ alone}$—$MFI_{Alexa\ 488+R18}$]/$MFI_{Alexa\ 488\ alone}$. **(B)** Reduction of Alexa 488 MFI (in %) on cells expressing CD8αβ WT (blue bars), CD8$\alpha\beta_{C137S}$ (red bars) or CD8$\alpha\beta_{C150S}$ (green bars). Mean values and SD were calculated from three experiments. **(C–E)** Alternatively the cells were incubated with $D^b$/P815 cells (E/T = 3/1) previously pulsed with the indicated concentrations of GP33 peptide variant KAVYNLATM. After 4 h the CD8αβ$^+$ P14 TCR$^+$ T cells (100%) were enumerated by flow cytometry on intracellular staining of IFNγ (C), TNFα (D) or surface staining of CD107A (LAMP1) (E). Mean values and SD were calculated from two or more experiments.

expression, compared with the CD8$\alpha\beta_{WT}$ transfectant (Fig. 3E). Thus, loss of the membrane proximal CD8$\alpha\beta$ interchain disulfide bond severely impaired the functional avidity of CD8$^+$ T cells and increased the CD8's Ig domain membrane proximity, whereas loss of the distal bond had the opposite effects and, in some instances, slightly increases T-cell response.

### CD8β stalk sialylation and MHC I expression increase CD8αβ Ig domain membrane proximity and inhibit T cell function

Based on the observation that extensive glycosylation and sialylation of conserved CD8β stalk threonines inhibits CD8 function and T cell activation [9,11,12,36,37], we hypothesized that interactions between negatively charged sialic acids and adjacent clusters of positively charged residues promote bending of the CD8 stalk distal to the CD8α$C_{151}$-CD8β$C_{137}$ disulfide bond and poise the CD8 Ig domain to bind pMHC on the T cell in *cis* (Fig. 4A and B).

To test this, we treated naive CD8$^+$ T cells with neuraminidase, to remove the negatively charged sialic acids, and assessed the membrane proximity of the CD8 Ig domain by means of donor fluorescence quenching. The cells were stained with Alexa 488 labeled anti-CD8β 53.5.81 Fab fragment alone or together with R18 and were analyzed by flow cytometry. Neuraminidase treatment decreased the Alexa 488 mean fluorescence intensity (MFI) by about 20% compared with untreated naïve T cells (Fig. 4C). To further examine how sialic acid residues, affect the proximity of the CD8 Ig domain membrane proximity, we used FRET measurements based on FLIM. The same cells were stained with Alexa 488 labeled Fab fragment of mAb 53.5.81 and the membrane dye DiD. The average FRET efficiency (*E*), reporting the distance between the CD8β Ig domain (donor) and the cell membrane (acceptor), was measured via change in fluorescence lifetime of the donor. The FRET efficiency decreased on neuraminidase treatment by approximately 17% (Fig. 4D). These results demonstrate that removal of negatively charged sialic acids decreases the CD8 Ig domain membrane proximity and argue that CD8-pMHC binding in *cis* is favored by sialylated O-linked sugars in the CD8β stalk.

In a complementary approach, we examined the membrane proximity of the CD8 Ig domain on CD8$\alpha\beta^+$ T cells expressing $K^b$ and $D^b$ (MHC$^+$) or not (MHC$^-$). To this end, we knocked down $K^b$ and $D^b$ on P14 TCR CD8$^+$ T cells bearing CD8$\alpha\beta_{WT}$, CD8$\alpha\beta_{C137S}$ or CD8$\alpha\beta_{C150S}$. Knockdown led to 95–97% reduction in $D^b$ or $K^b$ expression relative to untreated cells, while the expression of CD8α and CD8β was comparable in all groups (Fig. S5). The cells were labeled with Alexa 488 53.5.81 Fab with and without R18 and analyzed by flow cytometry (Fig. 4E and F). The reduction of the Alexa 488 fluorescence (MFI) in the presence of R18 was substantially lower on MHC$^-$ than on MHC$^+$ cells (Fig. 4G). Similar results were obtained when using FLIM-FRET. This indicates that knockdown of MHC I molecules decreased the CD8 Ig domain's membrane proximity. To test whether this would translate in functional effects, we examined whether reduced surface expression of MHC-I on CD8$^+$ T cells enhances their antigen recognition. MHC$^+$ or MHC$^-$ P14 TCR$^+$ CD8$^+$ T cells expressing CD8$\alpha\beta_{WT}$, CD8$\alpha\beta_{C137S}$ or CD8$\alpha\beta_{C150S}$ were incubated with $D^b$ transduced P815 cells that were pulsed with the LCMV GP33 peptide variant KAVYNLATM, and T-cell responses measured by intracellular IFNγ and TNFα staining. Both cytokine responses increased on $D^b$ and $K^b$ knockdown (Fig. 4H and I); a 25–30% increase was observed for the CD8$\alpha\beta_{C150S}$ expressing cells, while a more modest increase (8–12%) was detected for CD8$\alpha\beta_{C137S}$ expressing cells. These results indicate that knockdown of MHC I molecules and the CD8$\alpha\beta_{C137S}$ mutation decreased the CD8 Ig domain membrane proximity and enhanced T cell antigen recognition.

These results argue that CD8 binds to pMHC complexes on the same T cell. To directly test this, we labeled CD8 transduced T cell hybridomas with the cleavable cross-linker 3,3′-dithiobis(sulfosuccinimidyl propionate (DTSSP). After immunoprecipitation of MHC I molecules from detergent lysates and reducing SDS-PAGE, Western blotting revealed CD8α (Fig. S6A). Conversely, on immunoprecipitation of CD8, it revealed MHC I heavy chains (Fig. S6B). Mutation of CD8β C150 (CD8$\alpha\beta_{C150S}$) increased the amount of cross-linked CD8-pMHC complexes relative to wild type, whereas mutation of CD8β C137 (CD8$\alpha\beta_{C137S}$) decreased it. Consistent with our FRET data (Fig. 2A–D), these results demonstrated that CD8αβ associated with pMHC complexes on T cell hybridomas (in *cis*). Furthermore, we investigated CD8-pMHC association on activated, primary CD8$^+$ T cells by confocal microcopy. To this end cell-associated pMHC complexes were stained with Alexa 647 labeled anti $D^{b/d}/K^{b/d}$ mAb 34-1-2S and with FITC labeled anti-CD8β YTS 156 mAb. After incubation in the cold, the two fluorescent images showed a colocalization with a Pearson correlation coefficient of approximately 0.82 (1 = complete colocalization) (Fig. S6C). By contrast, when using the anti-CD8α mAb YTS 105, a colocalization of only about 0.14 was observed (Fig. S6D). A slightly higher colocalization (0.24) was observed when FITC labeled anti-CD71 mAb was used (Fig. S6E). Consistent with our and others biochemical experiments (Fig. S6A and B) [24,25,29], these results demonstrate that i) CD8αβ binds to pMHC I complexes on the same T cell and ii) the YTS 156, but not the YTS 105 mAb is permissive

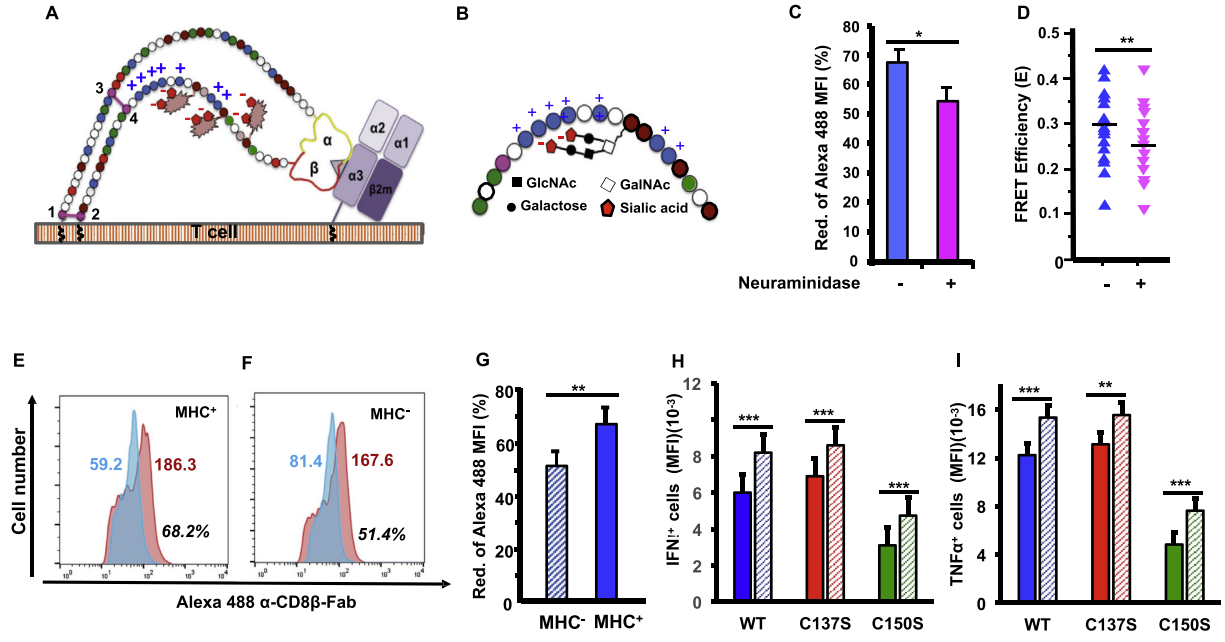


**Fig. 4. Desialylation and MHC I KO decrease CD8 Ig domain membrane proximity and increase CD8$^+$ T-cell responses. (A)** A cartoon representing CD8α (yellow) and CD8β (red) Ig domains and the CD8 stalks as chains of beads (amino acids) (color code: blue: basic; brown: conserved T; light brown: nonconserved T; magenta: C; green: P; red: D and E). On naive CD8$^+$ T cells the CD8β stalk carries negatively charged sialylated O-linked sugars (brown shapes and red pentagons for sialic acids), which undergo ionic interactions with adjacent positively charged CD8β sequences. Together with a distal interchain disulfide bond, CD8α$C_{151}$ (3) - CD8β$C_{137}$ (4) (magenta bar), these bend the CD8 stalks and poise the CD8 Ig domain (yellow and red shapes) to bind to pMHC (violet shapes) on the T cell (in *cis*). **(B)** Detail view of the CD8β stalk, showing threonines decorated with branched sugars, capped by negatively charged sialic acids undergoing ionic interactions with adjacent positively charged residues. **(C)** Naïve splenic CD8$^+$ T cells were treated (magenta bar) or not (blue bar) with neuraminidase and stained with Alexa 488 labeled anti-CD8β 53.5.81 Fab fragment with or without R18 and analyzed by flow cytometry. The reductions of Alexa 488 fluorescence (MFI in %) were calculated as described for Fig. 3A,B and the SD from four experiments. **(D)** Alternatively, the cells were stained with Alexa 488 labeled 53.5.81 Fab fragment and DiD and the proximity between the CD8β Ig domain and the cell membrane was measured as change in fluorescence lifetime of the donor (Alexa 488) in the presence of the membrane-located acceptor (DiD). Each dot represents the FRET efficiency (E) of a cell and the horizontal bars their mean values. **(E–F)** Sorted $D^{b-}K^{b-}$ (E) and $D^{b+}K^{b+}$ (F) P14 TCR$^+$ T cells were stained with Alexa 488 labeled 53.5.81 Fab fragment in the absence (red histograms) or presence (blue histograms) of octadecyl rhodamine B (R18) and analyzed by flow cytometry. The blue numbers indicate the Alexa 488 MFI in the presence and the red ones in the absence of R18 labeling; black numbers indicate the reduction of Alexa 488 MFI in presence of R18 and were calculated as described for Fig. 3A, B. **G.** The reductions of Alexa 488 MFI was assessed on sorted CD8αβ$^+$ $D^{b-}K^{b-}$ (MHC$^-$) and CD8αβ$^+$ $D^{b+}K^{b+}$ (MHC$^+$) cells and represented by a full and a hatched bar, respectively. Mean values, SD and p values were calculated from three experiments. **(H, I)** Splenocytes from CD8β KO, P14 TCR transgenic mice were transduced with CD8α cistronically linked to CD8β wild type (blue bars), CD8β$_{C137S}$ (red bars) or CD8β$_{C150S}$ (green bars) in the absence or presence of mirRNA targeting $D^b$ and $K^b$, respectively. After 10 days CD8αβ$^+$ $D^{b+}K^{b+}$ and CD8αβ$^+$ $D^{b-}K^{b-}$ cells were sorted and their IFNγ (D) and TNFα (E) responses assessed on incubation with P815 cells previously pulsed with 10 nM of KAVYNLATM peptide. The full bars indicate responses of MHC$^+$ and hatched bars of MHC$^-$ T cells. Mean values and SD were calculated from two experiments.

to CD8 binding to pMHC in *cis*, which proves, together with modeling, that binding in *cis* involves primarily the reversed docking orientation (Figs. S2A and B) [34].

## Biochemical analyses reveal two CD8αβ isoforms

Our results thus far indicate that CD8αβ exists in two forms: one containing a membrane distal disulfide bond, which favors an approximation of the CD8 Ig domain to the membrane and reduced availability to bind pMHC in *trans*, and the other lacking this posttranslational modification and favoring a greater distance from the membrane and increased availability of CD8 for binding pMHC in *trans*. We next assessed whether CD8 shows two biochemically different forms. We first examined T1.4 T cell hybridomas transfected with CD8β$_{WT}$, CD8β$_{C137S}$ or CD8β$_{C150S}$. After detergent lysis immunoprecipitated CD8 were analyzed on 8% nonreducing SDS-PAGE. Western blotting with

anti-CD8 mAb revealed that CD8$\alpha\beta_{WT}$ contained two species, migrating with apparent Mr of 73–75 kDa and 68–70 kDa, respectively (isoform 1 and 2) (Fig. 5A). Under reducing conditions CD8$\alpha$ migrated with an apparent Mr of about 38 kDa and CD8$\beta$ of 30 kDa, giving a Mr for CD8$\alpha\beta$ of 68 kDa. Isoform 2 was exclusively expressed on the CD8$\alpha\beta_{C150S}$ and isoform 1 on CD8$\alpha\beta_{C137S}^{+}$ hybridomas. This was observed irrespective of whether immunoprecipitation was performed with anti-CD8$\alpha$ or anti-CD8$\beta$ antibody. Free CD8$\beta$ was observed in case of the CD8$\alpha\beta_{C150S}$ mutant, indicating that the CD8$\alpha_{C151}$-CD8$\beta_{C137}$ interchain disulfide bond was not quantitatively formed or partially lost during the experiment. The same results were obtained when surface biotinylated CD8 was analyzed (Fig. S7A). The corresponding 12% reducing SDS-PAGE showed the expected CD8$\alpha$ and CD8$\beta$ chains (Figs. 5B,C and S7B,C). The heterogeneous bands observed in the CD8$\beta$ blots reflect heterogeneities in glycosylation and sialylation [9,11,12].

We then examined splenic CD8$^+$ T cells from P14 TCR$\beta$ chain transgenic mice that were infected or not with LCMV 8 days previously. Western blotting on 8% nonreducing SDS-PAGE with anti-CD8$\beta$ mAb revealed two CD8$\alpha\beta$ species, migrating with apparent Mr of 75–78 kDa and 70–73 kDa, respectively (isoform 1 and 2) (Fig. 5D), with nearly threefold more isoform 1 on T cells from uninfected mice, regardless of whether Western blotting was performed with anti-CD8$\alpha$ or anti-CD8$\beta$ antibody (Figs. 5D and S7). Conversely, the CD8 isoform 2 was slightly overexpressed on T cells from LCMV infected mice (Figs. 5D,F, S8A,C). The reducing gel showed the expected CD8$\alpha$ and CD8$\beta$ chains (Figs. 5E and S8B). The heterogeneous CD8$\beta$ bands reflect heterogeneities in glycosylation and sialylation. It is noteworthy that total CD8$^+$ splenic T cells from LCMV infected mice were used, some of which were not activated CTL.

## pMHC binding in *cis* attenuates CD8 coreceptor function

Our biochemical analysis and CD8 Ig domain membrane proximity measurements are consistent

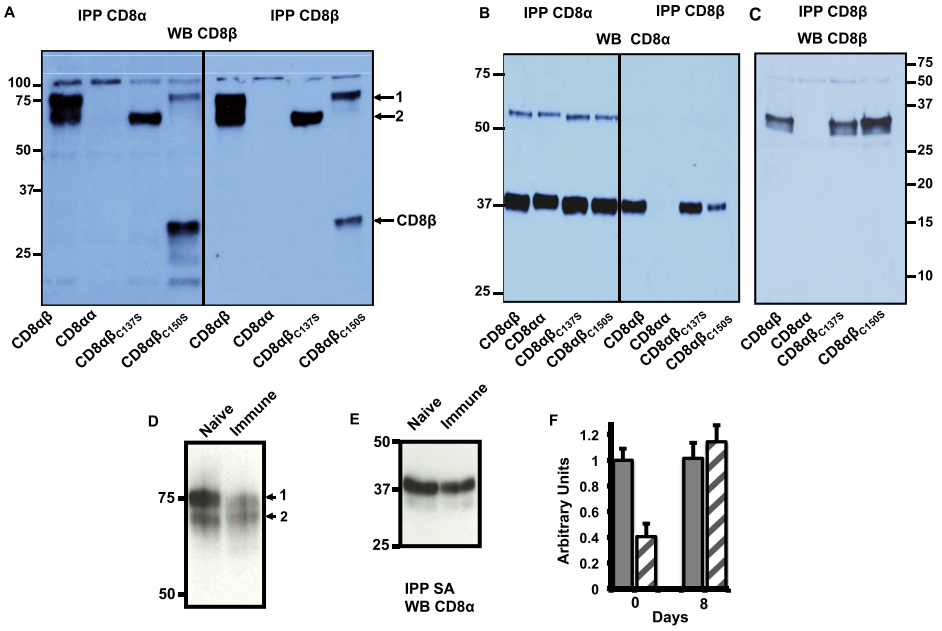


**Fig. 5. Interchain disulfide bonds define two CD8$\alpha\beta$ isoforms that affect T cell pMHC binding. (A)** T1.4 hybridomas expressing the indicated CD8 forms were lysed in n-octylglucoside (1%) containing buffer and CD8$\alpha$ (left side) or CD8$\beta$ (right side) immunoprecipitated, resolved on 8% nonreducing SDS-PAGE and Western blotted with anti-CD8$\beta$ mAb (WB KT112). The arrows indicate CD8 isoforms and the numbers the Mr standards in kDa. **(B, C)** The immunoprecipitates were resolved on 12% reducing SDS-PAGE and Western blotted with anti-CD8$\alpha$ (B) or anti-CD8$\beta$ (C) antibodies. Representative experiments out of six are shown. **(D–F)** The spleens of P14 TCR$\beta$ chain transgenic mice untreated (Naïve) or 8d post LCMV infection (Immune) were removed, their CD8$^+$ T cells isolated, surface biotinylated, detergent lysed, the isolated biotinylated molecules resolved on 8% nonreducing (D) or 12% reducing (E) SDS-PAGE and Western blotted with anti-CD8$\alpha$ antibody. The arrows indicate the CD8 isoforms 1 and 2. Molecular weight standards are indicated in kDa on the left side. Representative gels are shown out of three or more experiments. **(F)** Mean values and SD were calculated from densitometry readings of blots from three experiments and represented in bar graphs. Gray bars refer to CD8 isoform 1 and hatched bars to isoform 2 expressed on T cells from untreated (Naïve—day 0) or from LCMV immune mice (Immune—day 8).

with the view that there exists two CD8αβ isoforms; one of which lacks and the other has a membrane distal interchain disulfide bond, which infers different propensities for binding pMHC in *trans* and *cis*, respectively (Fig. 6A and B). An important feature of CD8αβ coreceptor function is to strengthen cognate pMHC binding by coengaging TCR-associated complexes. To directly measure this, T1.4 T cell hybridomas expressing $CD8\alpha\beta_{WT}$, CD8αα, $CD8\alpha\beta_{C137S}$ or $CD8\alpha\beta_{C150S}$ were incubated with soluble monomeric $K^d$/*IASA*-YIPSAEK(*ABA*)I complex and their binding to TCR was measured by TCR photoaffinity labeling (Fig. 6C) [4,5,8]. The highest labeling, i.e., binding was observed on T1.4 T cell hybridomas expressing $CD8\alpha\beta_{C137S}$ (Fig. 6D). By contrast, the labeling on T1.4 T cell hybridomas expressing $CD8\alpha\beta_{C150S}$ or CD8αα was over four- to fivefold lower compared with WT CD8. In the presence of Fab fragment of the anti-$K^d$ mAb SF1-1.1.1, which blocks CD8 binding to $K^d$ [8] TCR photoaffinity labeling was below 10% in all cases.

Finally, we reasoned that because pMHC complexes are excluded from lipid rafts, CD8 binding to pMHC in *cis* decreases its association with rafts and thus with Lck, which would not be the case when CD8 binds pMHC in *trans* (Fig. 6A and B)

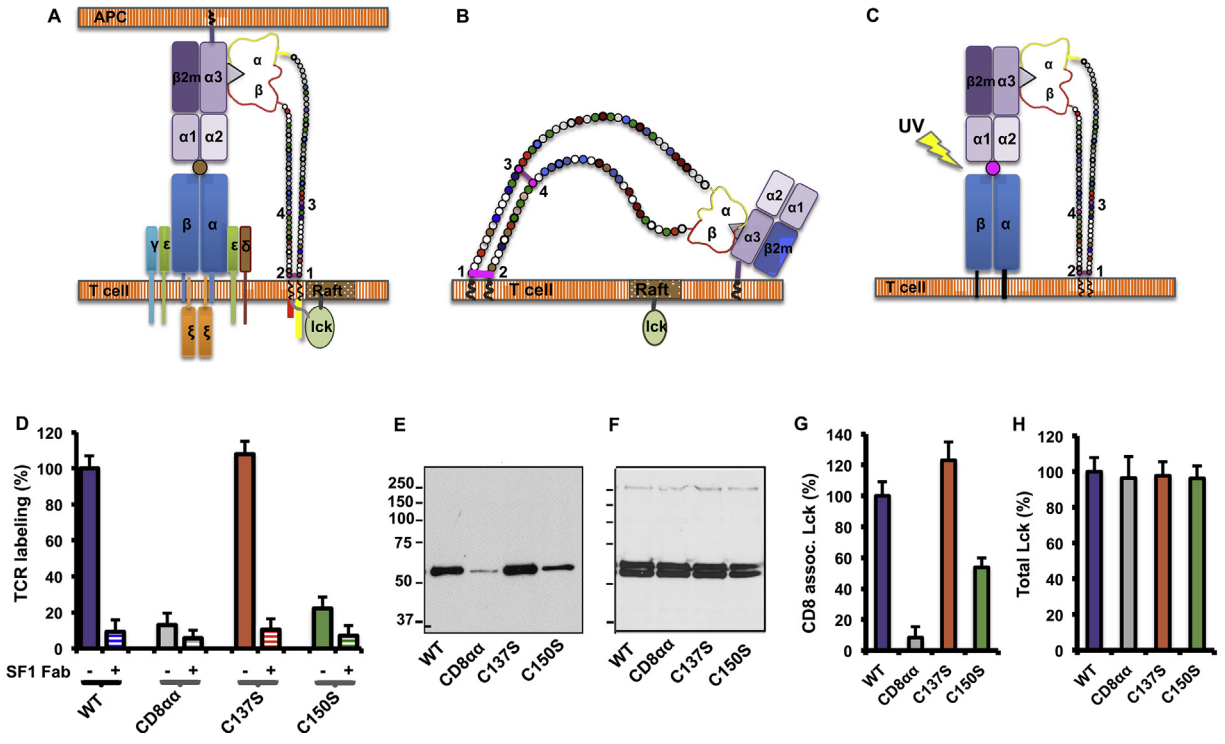


**Fig. 6. CD8-pMHC binding in *cis* negatively regulates CD8 coreceptor function. (A)** A cartoon of the coreceptor type CD8αβ-pMHC binding mode (in *trans*); the CD8 stalks have one interchain disulfide bond (magenta bar) between $CD8\alpha C_{166}$ (1) and $CD8\beta C_{150}$ (2) allowing an upright orientation and the CD8 Ig domain binding to cognate MHC (violet)-peptide (brown) complex on an antigen presenting cell (APC), engaged by TCRαβ (blue), associated with the CD3ϵδ (green and light blue), CD3ϵγ (green and brown) and CD3ξξ (orange). CD8 is associated with lipid rafts (brown shape) and $p56^{Lck}$ (Lck) (green shape) and is active as coreceptor. **(B)** Cartoon illustrating CD8 inactivation by binding to pMHC (violet shapes) in *cis*. Because MHC I molecules are excluded from lipid rafts (brown shape) this interaction decreases CD8-Lck association. **(C)** Cartoon illustration TCR photoaffinity labeling. Soluble MHC (violet) containing a photoreactive peptide (magenta) was incubated with T cell hybridomas and UV irradiated; the covalently cross-linked TCR (blue)-pMHC complexes were immunoprecipitated and quantified. **(D)** T1.4 T cell hybridomas expressing CD8αβ wild type (WT) (blue), CD8αα (gray), CD8αβC137S (C137S) (red) or CD8αβC150S (C150S) (green) were incubated at 26 °C for 60 min with soluble $K^d$-$^{125}$*IASA*-YIPSAEK(*ABA*)I monomer in the absence (fully bars) or presence of Fab fragments of the anti-$K^d$ antibody SF1-1.1.1 (stripped bars); after UV irradiation the covalent pMHC-TCR complexes were quantified. Mean values and SD were calculated from three experiments; 100% refers to the value observed for the CD8αβ WT hybridoma. **(E–H)** T1.4 hybridomas expressing CD8αβ (WT), CD8αα, $CD8\alpha\beta_{C137S}$ (C137S) or $CD8\alpha_{C150S}$ (C150S) were lysed in Brij 78 detergent (1%) and CD8β (F) or Lck (G) immunoprecipitated. The immunoprecipitates were resolved on SDS-PAGE (10% reducing) and Western blotted with anti-Lck antibody. Molecular weight standards are indicated in kDa. The Lck blots were quantified and represented in bar graphs using the same color-coding as in D (H, I). Hundred percent refers to wild type CD8αβ. Mean values and SD were calculated from three experiments.

[4,5,38–40]. To test this, we assessed the association of CD8 with Lck on the T cell membrane. We immunoprecipitated CD8β (Fig. 6E) or Lck (Fig. 6F) from T1.4 hybridomas expressing $CD8\alpha\beta_{WT}$, CD8αα, $CD8\alpha\beta_{C137S}$ or $CD8\alpha_{C150S}$ and under reducing conditions Western blotted with anti-Lck antibody. We observed that the CD8 association with Lck was increased by the $CD8\alpha\beta_{C137S}$ mutation, but decreased by the $CD8\alpha\beta_{C150S}$ mutation (Fig. 6G–H). These results taken together support the view that the membrane distal inter-chain disulfide bond defines a CD8αβ configuration that promotes CD8 IgG domain membrane proximity and inhibits CD8 function by favoring CD8 binding to pMHC on the T cell (in *cis*).

## Discussion

The stalks of CD8α and CD8β are remarkably different in length, glycosylation and charge patterns and positioning of their cysteines, all of which are evolutionary conserved traits (Fig. 1A–C). Replacing the CD8α stalk with the one of CD8β or vice versa has dramatic effects [41,42]. CD8αβ binding to cognate pMHC complexes in the coreceptor configuration on another cell [17] or to pMHC on the same T cell may involve different docking modes, which is similar to what has been shown for Ly49 (Fig. 1F–H) [24–28]. Our modeling identified a stable CD8αβ-$K^b$ complex, in which the CD8 Ig domain is approximately 180° rotated compared with the known complexes (Fig. 1D–H) [17]. In the reversed orientation, contacts are formed between CD8α and $K^b$ α2 domain and adjacent $K^b$ α3 domain residues that are not found in the coreceptor type structure (Fig. 1H and I, Table 1). Indeed, mutations of the predicted $K^b$ α2 contact residues inhibited the adhesion of $CD8^+$ T cells to immobilized $K^b$-peptide complexes by about 37% (Fig. 1J and K).

Before the CD8αβ-$D^d$ structure was elucidated, mutational analyses were performed to identify the orientation of CD8αβ binding to pMHC, which suggested the existence of two CD8-pMHC docking modes [20–23]. Indeed, the X-ray structure of the *trans* CD8-$D^d$ complex failed to explain the effect of several mutations, most of which are explained by our modeled CD8-pMHC complex in the reversed orientation (Fig. 1H and I, Table 1) [17]. For example, mutation of CD8α R8 and E27 showed strong effects on T cell hybridomas and $CD8^+$ T cell thymic selection [21,43]. In our model these residues made contacts with $K^b$ α2 residues, which is not the case in the CD8αβ-$D^d$ structure. Furthermore, in our model the CD8α residues S31, Q34, and S108 made contacts with distal MHC α3 residues (Table 1), which was also the case in the CD8αα-$K^b$, but not in the CD8αβ-$D^d$ X-ray structure, demonstrating that there exist a CD8αβ-pMHC complex in which CD8α is positioned proximal to the MHC variable domain [17,19–23]. CD8 contacts with the MHC variable domains are also strongly suggested by the MHC allele specificity of CD8-pMHC binding, because the polymorphism of MHC molecules is found mostly in their variable domains [9,44]. Furthermore, the existence of a second, reversed CD8-pMHC binding mode was demonstrated by antibody blocking experiments, such as: i) the anti-CD8α mAb 53.6.72 blocks CD8-mediated T cell adhesion, but not cognate pMHC binding, indicating that there exist two different CD8-pMHC binding modes (Fig. S2E) [8,35]; ii) the anti-CD8β mAb YTS 156 showed colocalization with pMHC complexes on T cells, whereas the anti-CD8α mAb YTS 105 did not, which together with modeling and the observation that the former mAb blocked the coreceptor-like and the latter the reversed CD8-pMHC binding mode (Figs. S2A–D and S6C,D), demonstrates that *cis* binding involved the reversed CD8αβ orientation on the MHC [17,33,34].

We observed opposing effects of serine mutations of the membrane proximal (C150) and distal (C137) CD8β cysteines on structure and function of the coreceptor (Figs. 2 and 3). However, the reduced $Ca^{2+}$ flux and cytokine responses of transduced T cell hybridomas and primary activated T cells observed for the $CD8\beta_{C150S}$ mutation may in part be explained by reduced CD8 surface expression (Figs. S3 and 4). Indeed, the corresponding $CD8\alpha_{C166S}$ mutation caused impaired CD8α-CD8β chain assembly and intracellular transport to the cell surface [18]. On the other hand, mutation of the membrane distal cysteines ($CD8\alpha_{C151S}$ and $CD8\beta_{C137S}$) had no apparent effect on CD8 surface expression (Figs. S3 and 4) [18] and the increase in T-cell responses observed for the $CD8\beta_{C137S}$ mutation suggested that the distal interchain disulfide bond has regulatory properties (Figs. 2E,F and 3C–E). This increase was underestimated, because a substantial fraction of the reference wild type CD8 lacked this bond, as seen by the appearance of free CD8β on nonreducing SDS-PAGE on serine mutation of CD8β C150, which removed the membrane proximal disulfide bond ($CD8\alpha_{C166S}$ and $CD8\beta_{C150S}$) (Figs. 5A and S7A). Moreover, disrupting this disulfide bond substantially reduced the average membrane proximity of the CD8 Ig domain, which plausibly explains the increase in T cell reactivity, because CD8 to act as coreceptor needs to be in a fully extended configuration (Figs. 2, 3 and 6A) [17]. The CD8αα stalk has an extended and semirigid structure [15,16], but for the CD8β stalk all that is known is that it is 8–10 residues shorter and that there are 2–4 residues fewer between its two cysteines (Fig. 1A–C) [9]. If these form two interchain disulfide bonds, this asymmetry predictably infers a kink in the CD8 stalk, thus bringing the CD8 Ig domain closer the membrane (Figs. 2A–D,

3A,B and 6B). It is interesting to note that proline residues are located N-terminal of the distal stalk cysteines (Figs. 1A,B, 4A and 6A,B). Proline has low *cis-trans* isomerization energy and therefore is often found in bends and hinge regions [45,46].

Because of the long and semirigid nature of the CD8 stalks and the asymmetric positioning of their distal cysteines, the CD8$\alpha C_{151}$-CD8$\beta C_{137}$ interchain disulfide bond is expected to infer major conformational changes. We suggest that the two CD8 isoforms observed on nonreducing gels reflect this, i.e., that the difference in electrophoretic mobility is accounted for by the presence (isoform 1) or absence (isoform 2) of the membrane distal interchain disulfide bond (Figs. 5A,B and S7A). These changes were linked to CD8 function. The CD8$\beta_{C137S}$ mutation increased T-cell responses, whereas the CD8$\beta_{C150S}$ mutation decreased it (Figs. 2E,F and 3C–E). In accordance with this, the inactive CD8 isoform 1 was dominant on naïve T cells, which are poorly antigen reactive, whereas the active isoform 2 was abundant on activated CD8$^+$ T cells, which are highly antigen reactive (Figs. 5D–F and S8) [12,13]. Taken together, our results indicate that the presence of the membrane distal interchain disulfide bond substantially increased the proximity of the CD8 Ig domain to the cell membrane, thus favoring CD8 binding to pMHC on the T cell in *cis* (Figs. 2 and 3). The more CD8 binds to pMHC on the T cell (*cis*), the less CD8 is available for binding to pMHC molecules on another cell (*trans*), which is required for CD8 coreceptor function (Fig. 6A and B) [17]. A similar negative regulatory principle governs Ly49s activity and NK function [26–28].

It remains to be explained how CD8 function, namely interchain disulfide bond formation, is regulated. It is known that T cell development and differentiation involves changes in the glycosylation and sialylation of threonines in the CD8$\beta$ stalk and that these modulate thymocytes and T cell reactivity [10–14,36]. These changes have been proposed to alter the binding affinity of CD8 for pMHC via conformational changes [9], a view that has been questioned later [15]. Our data suggest that these changes modulate T cell reactivity by altering the proportion of the activating and inactivating CD8 isoforms (Figs. 2, 3 and 5). The CD8$\beta$ stalk shows clusters of positively charged residues distal to the second cysteine and adjacent to threonines whose glycosylation changes on T cell differentiation (or thymocyte maturation) (Fig. 1A and B). We propose that this enables interactions between negatively charged sialic acids and positively charged residues, which "bend" the CD8 stalk (Fig. 4A and B). As a result, the CD8 Ig domain becomes membrane proximal and poised to bind pMHC on the T cell. Indeed, our FRET and fluorescence quenching experiments showed that the membrane proximity of the CD8 Ig domain was decreased by both enzymatic sialic acid removal and MHC knockdown (Fig. 4C–G). These treatments increased T-cell responses, corroborating the view that CD8 binding pMHC in *cis* is a negative regulatory principle (Figs. 4H,I and 6A,B) [9–13,36]. This is consistent with the observation that CD8$\alpha\beta$ is exceptionally active on double positive thymocytes, which have very low MHC I expression [47,48]. This has translational relevance, as it has been shown that CD8$^+$ T cell reactivity and tumor control requires CD8$\beta$ desialylation or sialic acid blockade [37,49,50].

The interdependence between the CD8 isoforms and changes in CD8 glycosylation and sialylation remain to be elucidated. Conceivably, formation of the distal CD8 interchain disulfide bond (isoform 1) requires CD8$\beta$ to be fully glycosylated and sialylated, i.e., to assume a bent configuration. However, other factors may be involved as well. For example, CD8$^+$ T cell priming increases thiol expression and disulfide exchange reactions [50,51], which may promote reduction of the distal CD8 interchain disulfide bond. Indeed, T cells with high thiol surface expression show high antitumor activity [52]. It is important to note, however, that T cells (and thymocytes) depending on their stage of differentiation and development can express different glycans, and that these can affect and CD8 function and T cell reactivity in diverse ways [15,53–56].

We have established that binding of CD8 to pMHC on the T cell inhibits T cell activation and thus is a means to tune CD8$^+$ T-cell responses (Figs. 2–4). In addition, for efficient activation of CD8$^+$ T cells, CD8 needs to coengage TCR-associated cognate pMHC complexes and bring active Lck to the TCR/CD3, which both are spoiled by CD8 binding pMHC in *cis* (Fig. 6). Indeed, because pMHC complexes are excluded form lipid rafts, CD8 binding to pMHC on the T cell decreases CD8-association with Lck, which in turn diminishes CD8 function (Fig. 6E–H) [4–6,38–40]. Available evidence argues that this novel negative regulatory principle is induced on one hand by negatively charged glycans in the CD8 stalks and by the presence of membrane distal CD8 interchain disulfide bond on the other (Figs. 2–4) [13,36,37].

In conclusion, we showed that CD8 function and hence CD8$^+$ T cell reactivity was inhibited by CD8 binding to pMHC on the T cell (in *cis*) in the reversed orientation. This inhibition was regulated by post-translational changes of the CD8 stalk that altered its configuration and CD8 function by balancing CD8-pMHC binding in *cis* or *trans* (Figs. 2–4). Ligand binding in *cis* versus in *trans* is a means to regulate the activity of different receptors, such as Ly49s, Notch, the sialic acid-binding receptors siglec-G, CD22 and neurophilin 1 [56]. Similar to CD8, several Ly49s can bind pMHC in *cis* and *trans*, respectively, which requires structural changes in the Ly49 stalk

[26–28]. Negative regulation of CD8 function serves to tune $CD8^+$ T cell reactivity and apoptosis [13,14,52,53]. This negative regulation is exploited by tumors to avert immune attacks [37,49]. Our findings provide new perspectives for T cell engineering in translational settings.

## Materials and Methods

*Antibodies*— Monoclonal anti-CD8α 53.6.72, anti-CD8β H35-17, anti-TCRβ H57 and anti-CD45.1 A20.1 were from the American Type Culture Collection (ATCC); the anti-CD8β 53.5.8 and KT112 mAb were a gift from Dr. Eichmann, (Max Planck Institute, Freiburg); rabbit anti-CD8α was from Antibodies-online.com and anti-Lck clone 3A5 from Santa Cruz Biotechnology.

*CD8 transfected T1 T cell hybridomas*— Mouse CD8β cDNA was introduced into the pSP72 cloning vector (Promega) and mutated using two-steps nested PCR. The $CD8\beta_{C137S}$ and $CD8\beta_{C150S}$ mutants were sequenced using T7 and SP6 universal primers. The [*BamHI-XhoI*] fragments carrying wild type or mutant CD8β ORF were subcloned into the [*BamHI-SalI*] open pMI expression vector, which contained a human CD2 reporter gene [57]. The $CD8\alpha^+$ T1.4 cell hybridoma was a gift from Dr. Malissen, CIML, Marseilles) and was cultured in DMEM containing 5% FCS, 50 μg/ml penicillin, 50 μg/ml streptomycin, 100 μg/ml neomycin, 50 μM β-mercaptoethanol, 4 mg/ml of G418 (Calbiochem, San Diego, CA), as described [5]. Retroviral gene transfer was as follows: the CD8β-carrying pMI plasmids were first introduced into the Phoenix ϕNX-A retrovirus packaging cell line via calcium phosphate precipitation [57]. The resulting supernatants were used to transfect the $CD8\alpha^+$, $CD8\beta^-$ T1.4 hybridoma. After four days the transfected hybridomas were FACS-sorted for high CD8α and CD2 expression, cultured in DMEM and FACS-cloned for high CD2 expression.

*TCR and CD8 cotransduction of splenocytes*— Retroviral transfer of CD8 and TCR genes were performed essentially as described [58,59]. In brief, $CD3^+$ splenocytes from P14 TCR transgenic, CD8βKO mice were stimulated with Dynabeads containing mouse anti-CD3 and CD28 antibodies (ThermoFisher) for 24 h in the presence of IL-2 (20 U/ml) (Roche). Retroviral supernatants were added in RetroNectin precoated 24-well plates and centrifuged for 90 min at 2000-x g and 32 °C. Stimulated T cells were added into the plates and after overnight incubation; retroviral supernatant was replaced by fresh medium containing IL-2 (20 U/ml). After 5 d IL-15 (12 U/ml) was added to preserve $CD8^+$ T cells and loose $CD4^+$ T cells. The Dynabeads were removed 8 d post transduction. The cotransduced $CD8^+$ T cells were used 12d post transduction. Retroviruses were produced by means of Phoenix Eco cells cultured in T150 flasks and transfected with 14.3 μg pCL-eco packaging plasmid and 21.4 μg target plasmid using TurboFect Transfection kits (ThermoFisher). Viral supernatants were harvested after 48 h and centrifuged at 20,000-x g for 2 h. The pellet was resuspended in 400 μL RPMI 1640 medium.

*Knockdown of $D^b$ and $K^b$*—For the miR coexpression the NeoR/KanR-IRES-ZsGreen1 cassette from the pLMN vector (https://www.biocat.com/shrna/shrna-sets/TRMSU2000-14972-GVO-TRI) was replaced by the CD8 variants under study. The shRNA included in the miR-30 backbone is acgacgcggagaatccgagata. The gene 14972 designates mouse H2-K and D census H-2 histocompatibility sequences. We used dual-target shRNA of Db and Kb, and CD8β variants in primary CD8α+ T cells from CD8β KO, P14 TCR transgenic mice. After 10 days of transduction, $CD8\alpha\beta^+D^{b+}K^{b+}$ and $CD8\alpha\beta^+D^{b-}K^{b-}$ cells were FACS sorted and analyzed by flow cytometry and FRET.

*Flow cytometry and intracellular $Ca^{2+}$ and cytokine measurements*— T cell hybridomas were washed in PBS and resuspended at $2 \times 10^6$ cells/ml in serum free OptiMEM medium (Life Technologies, Merebeke, Belgium) containing 1% BSA (FACS buffer). For intracellular $Ca^{2+}$ mobilization measurments P815 cells ($1 \times 10^6$ cells/ml) were pulsed with graded concentrations of PbCS(ABA) (SYIPSAEK(*ABA*))I peptide for 1 h at 37 °C and incubated with T cell hybridomas ($1 \times 10^6$ cells/ml) previously labeled with 5 μM indo-1 (Sigma, Buchs, Switzerland) at 37 °C for 45 min. After incubation for 2 min at 37 °C at an E/T ratio of 1/3, $Ca^{2+}$ dependent Indo-1 fluorescence was measured on a LSR II (BD) and IL-2 release by T cell hydridomas was assessed as described [4,5]. Intracellular cytokine staining of IFNγ and TNFα in primary T cells was performed as described previously [60].

*FRET measurements by fluorescent microscopy*—For FRET experiments Alexa 488 Fab fragments were produced as follows: anti-CD8β mAb 53.5.81 (rat IgG1) purified on protein-G sepharose (Amersham, GE Health Science) was digested with pepsin for 2 h at 37 °C (Pierce Chemical Co., Rockford, IL, USA) followed by dialysis against PBS at 4 °C overnight. The resulting $(Fab)_2$-fragments were reduced with 20 mM of cysteamine in 10 mM EDTA for 1 h at 37 °C and the resulting Fab fragments (2.5 mg) incubated with of with 150 mmol of Alexa 488 maleimide (Invitrogen) for 2 h at ambient temperature. Excess of Alexa 488 maleimide was removed by dialysis against PBS at 4 °C overnight. For FRET experiments T1.4 hybridoma expressing CD8αβ, $CD8\alpha\beta_{C137S}$ or $CD8\alpha\beta_{C150S}$ were incubated with 12 μm/ml of Alexa Fluor 488-labeled 53.5.81 anti-CD8β Fab fragment in PBS containing 5% FCS for 30 min on ice. After one wash with PBS the cells were incubated with 5 μM of DiD (1 mM stock solution in DMSO; Life Technologies) in PBS for 5 min at room temperature. After one wash the cells were imaged in LabTek 8-chamber coverslips (NUNC, Rochester, NY) using a confocal inverted Olympus IX71 microscope (Olympus, Hamburg, Germany). Fluorescent probes were excited by pulsed laser diodes LDH-P-C-470 and LDH-D-C-635, PicoQuant, Berlin, Germany operating at 20 MHz. Possible bleak-through effects were eliminated by alternating excitation using low output power. The laser light from both lasers was coupled to an optical fiber, collimated by an air space objective (UPLSAPO 4X, Olympus) and up reflected to a water immersion objective (UPLSAPO 60x, Olympus) with a 470/635 dichroic mirror. The emission light was split on two avalanche photo diodes by a 635 dichroic mirror and 515–550 nm and 697–758 nm band filters (Chroma Rockingham, VT) for Alexa Fluor 488 and DiD, respectively. The detectors were connected to two independent electronic circuits of HydraHarp, PicoQuant,

Germany. Each of the 512 × 512 pixels contained information on individual photon arrival times with a subnanosecond time resolution. If sufficient photons per pixel are collected, time-resolved histograms for individual pixels can be obtained. The FRET efficiency, *E*, was calculated as described previously [61], i.e.,

$$E = 1 - \frac{\langle \tau_{DA} \rangle}{\langle \tau_D \rangle} = 1 - \frac{\int_0^\infty t F_{DA}(t)}{\int_0^\infty t F_D(t)}$$

where $\langle \tau_D \rangle$ and $\langle \tau_{DA} \rangle$ are average donor and donor-acceptor fluorescence lifetimes and $F_{DA}(t)$ and $F_D(t)$ indicate the time-resolved fluorescence intensities in the presence or absence of FRET, respectively. To calculate *E* only photons emitted from the plasma cell membrane were analyzed. This was achieved by selecting pixels for the analysis that i) contained signal from the membrane and ii) were displayed by means of the phasor plot approach (see below) to the center of a cluster that corresponds to the donors undergoing FRET within the cell membrane. The diameter of the cluster center was set to 256 ps in this study. The phasor approach [62] is based on calculating the following coordinates for every pixel:

$$\begin{bmatrix} \mathrm{Re} \\ \mathrm{Im} \end{bmatrix} = \frac{1}{\sum_{i=1}^{L} I_i} \begin{bmatrix} \sum_{i=1}^{L} I_i \cos \frac{2\pi n}{L}(i - i_0) \\ \sum_{i=1}^{L} I_i \sin \frac{2\pi n}{L}(i - i_0) \end{bmatrix}$$

where $I_i$ is fluorescence intensity in the *i*th time-correlated single photon counting (TCSPC) channel, *L* the number of TCSPC channels, *n* is an arbitrarily chosen integer (here $n = 4$) corresponding to the frequency in the Fourier space, $i_0$ is a channel position of the decay rising edge; $i_0$ is commonly determined by measuring TCSPC histogram of a single exponential dye (fluorescein). The calculation is followed by construction of a 2D histogram of *Re* and *Im* coordinates. Individual clusters in the phasor plot correspond to various spatially resolvable decay functions.

*TCR photoaffinity labeling*—T cell hybridomas ($7 \times 10^6$ cells/ml) were incubated in a 12 well plates with $K^d$-$^{125}$*IASA*-YIPSAEK(*ABA*)I ($0.5–1.5 \times 10^7$ cpm/$5 \times 10^7$ cells). After 1 h of incubation at 26 °C and UV irradiation at 312 ± 40 nm for 30 s with 90 W, the cells were washed twice and lyzed for >60 min on ice in 1 ml PBS containing 1% n-octylglucoside and a mixture of protease inhibitors (Roche, Rotkreuz, Switzerland). TCR was immunoprecipitated using H57-coupled Sepharose beads. The immunoprecipitates were resolved on SDS-PAGE (10% reducing) and radioactivity was quantified by phosphoimaging using a Fuji BAS1000 PhosphorImager [8].

*Immunoprecipitation and Western blotting*— T cells ($5 \times 10^7$ cells) were washed in PBS supplemented with 1 mM $MgCl_2$ and 0.1 mM $CaCl_2$ and incubated or not with 0.2 mg/ml sulfosuccinimidyl 6-biotinamido-hexanoate (sulfo-NHS-LC-biotin, Pierce) for 30 min at 4 °C under agitation. After addition of 5% FCS for 10′ at 4 °C, cells were washed twice in PBS. The cells were lyzed on ice for 1 h in 2 ml lysis buffer (20 mM Tris, pH 8.0; 150 mM NaCl, 5 mM iodoacetamide, 1% n-octylglucoside and protease inhibitors (Roche)). The lysates were centrifuged at 12,000 rpm for 15 min and the supernatants incubated for 30 min at 4 °C with Sepharose beads. The supernatants were incubated under agitation overnight at 4 °C with H35, 53.6.72 or 3A5 antibody conjugated Sepharose 4B beads. Alternatively, biotinylated molecules were recovered by overnight incubation at 4 °C with monomeric-avidin ultralink resin (Pierce, ThermoFisher Scientific). After three washes with buffer containing 20 mM Tris, pH 8.0; 500 mM NaCl and 1% TritonX and protease inhibitors (Roche), the immunoprecipitates were eluted with 40 µl Glycine buffer (0.1 M, pH 3.0), neutralized with 4 µl Tris buffer (1 M, pH 8.0), boiled in Laemmli buffer (±5% β-mercaptoethanol) and resolved on SDS-PAGE, transferred onto nitrocellulose membrane and labeled using antibodies. For detection the enhanced chemoluminescence (ECL, Amersham-Pharmacia) was used as recommend by the supplier. Isolation of $CD8^+$ splenocytes from naïve or LCMV-infected P14 TCRβ chain transgenic mice was performed as described previously [61].

*Modeling the CD8αβ-$K^b$ complexes*— An initial structure of the CD8αβ-$K^b$ complex in the reverse orientation was constructed based on the X-ray structure of the CD8αα-$K^b$ complex[19] (PDB 1BQH). The structure of the CD8αβ immunoglobulin domain was taken from the X-ray structure of the CD8αβ-$D^d$ complex [17] (PDB 3DMM). Using USCF Chimera [63] we superimposed CD8α and CD8β of CD8αβ to the MHC variable domain-proximal and distal CD8α entities of CD8αα, respectively. Starting with this initial structure, sets of contact residues were identified in both $K^b$ and CD8αβ. We then performed protein-protein docking using the HADDOCK software [31,32]. Ambiguous distance restraints (satisfied if any nonspecified subset of interatomic distances between two molecular regions is low) were applied to approximately define the target interface regions, without restricting the CD8 binding orientation. We followed the standard HADDOCK protocol and stared from random orientations of the dissociated molecules; 3000 complex structures were generated using rigid body energy minimization, out of which 300 were refined using semiflexible simulated annealing; 200 were further refined in the presence of solvent molecules. Final refined structures were clustered using an RMSD cutoff of 5 Å. An independent docking of CD8αβ to $D^d$ starting from the 3DMM structure (coreceptor orientation) yielded qualitatively similar results (Fig. S1), indicating that docking orientations obtained do not depend on the initial CD8αβ orientation or on the MHC allele. The best-scoring CD8αβ-$K^b$ docking poses in the coreceptor-like and reverse orientation were used to construct models of these complexes bound to the YTS105.18 or YTS156.7.7 Fab. As templates, we used the X-ray structures of the Fab bound to CD8αα (PDB 2ARJ) [33] and CD8αβ (PDB 3B9K) [34], respectively. In each case, the CD8 chain closest to the Fab in the CD8-Fab crystal structure was superimposed with the corresponding CD8 chain in the CD8αβ-$K^b$ model using UCSF Chimera.

## Confocal Microscopy

Isolated $CD8^+$ splenocytes from C57BL/C mice were incubated in anti-CD3 and anti-CD28 coated plates for 24 h. The activated CD8 T cells were washed in PBS (2×) and incubated on multiport microscope slides in serum-free IMDM medium at 37 °C for 30 min to allow CD8 T cell adhesion onto glass slides. The cells were fixed with 4% PFA at RT for 20 min, washed with PBS and incubated with PBS containing 1% BSA in at RT for 15 min. After washing with PBS (3×), cells were incubated with anti-FITC labeled CD8β mAb YTS 156 or anti-CD8α YTS 105 together with APC labeled anti-$D^{d/b}/K^{d/b}$ mAb 34-1-2S-APC (3 μg/ml for 1 h on ice). After washing the samples were mounted, sealed and examined with a Zeiss LSM 710 confocal microscope and images were recorded in multitracking mode. Colocalization analysis was performed using the Pearson coefficient method in the Fuji software.

### Statistics

Results were expressed as mean ± the standard deviation SD. Statistical analysis was performed using GraphPad Prism (version 7; San Diego, CA, USA). Nonparametric data sets were determined by one-way ANOVA test with two-tailed $p$ value. Parametric data sets were determined by two-way ANOVA test. $p$ values of 0.05 or less were considered as statistically significant. Significance levels: $^*p \leq 0.05$; $^{**}p \leq 0.01$; $^{***}p \leq 0.001$; $^{****}p \leq 0.0001$.

## CRediT authorship contribution statement

**Yang Liu:** Investigation, Formal analysis. **Michel A. Cuendet:** Methodolgy, Writing - review & editing. **Laurence Goffin:** Investigation. **Radek Šachl:** Investigation. **Marek Cebecauer:** Investigation. **Luca Cariolato:** Validation. **Philippe Guillaume:** Resources. **Patrick Reichenbach:** Investigation. **Melita Irving:** Supervision. **George Coukos:** Supervision, Resources. **Immanuel F. Luescher:** Supervision, Writing - original draft.

## Acknowledgments

A part of this study was supported by the Swiss National Science Foundation Grant 310030_12533/1, by the Czech Science Foundation (MC: 15-06989S and RŠ 18-04871S), and the Ludwig Institute for Cancer Research. The authors gratefully acknowledge helpful assistance by Dr. Nahzli Dilek.

## Appendix A. Supplementary data

Supplementary data to this article can be found online at https://doi.org/10.1016/j.jmb.2019.10.019.

*Received 2 July 2019;*
*Received in revised form 21 October 2019;*
*Accepted 23 October 2019*
Available online 5 November 2019

***Keywords:***
CD8;
MHC;
Structure;
T-cell receptor;
T cell

†These authors have contributed equally.

***Abbreviations used:***
Alexa 488, Alexa flour 488 dye; *ABA*, 4-azidobenzoic acid; DiD, 1,1′-dioctadecyl-3,3,3′,3′-tetramethylindodicarbocyanine 4-chlorobenzenesulfonate; Fab, Fragment antigen binding; FLIM, fluorescence lifetime imaging microscopy; FRET, Fluorescence resonance energy transfer; *IASA*, iodo, 4-azido salicylic acid; $K^b$, H-$2K^b$; Lck, lymphocyte-specific protein tyrosine kinase; LCMV, Lymphocytic choriomeningitis virus; mAb, monoclonal antibody; MFI, Mean fluorescence intensity; MHC I, major histocompatibility complex class I; Mr, Molecular weight; PAGE, Polyacrylamide gel electrophoresis; PbCS, Plasmodium *berghei* sporozoite protein; PbCS(*ABA*), YIPSAEK(*ABA*)I; pMHC, peptide MHC I; R18, octadecyl-rhodamine B; RMSD, Root mean square deviation; SDS, Sodium dodecyl sulfate; TCR, T-cell antigen receptor; WT, Wild Type.

## References

[1] E.L. Reinherz, J.H. Wang, Codification of bidentate pMHC interaction with TCR and its co-receptor, Trends Immunol. 36 (2015) 300–306.
[2] V. Renard, P. Romero, E. Vivier, B. Malissen, I.F. Luescher, CD8 beta increases CD8 coreceptor function and participation in TCR-ligand binding, J. Exp. Med. 184 (1996) 2439–2444.
[3] P.W. Kim, Z.Y. Sun, S.C. Blacklow, G. Wagner, M.J. Eck, A zinc clasp structure tethers Lck to T cell coreceptors CD4 and CD8, Science 301 (2003) 1725–1728.
[4] A. Arcaro, C. Grégoire, N. Boucheron, S. Stotz, E. Palmer, B. Malissen, I.F. Luescher, Essential role of CD8 palmitoylation in CD8 coreceptor function, J. Immunol. 165 (2000) 2068–2076.
[5] A. Arcaro, C. Grégoire, T.R. Bakker, L. Baldi, M. Jordan, L. Goffin, N. Boucheron, F. Wurm, P.A. van der Merwe, B. Malissen, I.F. Luescher, CD8beta endows CD8 with

efficient coreceptor function by coupling T cell receptor/CD3 to raft-associated CD8/p56(lck) complexes, J. Exp. Med. 194 (2001) 1485–1495.
[6] R. Bosselut, S. Kubo, T. Guinter, J.L. Kopacz, J.D. Altman, L. Feigenbaum, A. Singer, Role of CD8beta domains in CD8 coreceptor function: importance for MHC I binding, signaling, and positive selection of CD8+ T cells in the thymus, Immunity 12 (2000) 409–418.
[7] M.A. Doucey, D.F. Legler, N. Boucheron, J.C. Cerottini, C. Bron, I.F. Luescher, CTL activation is induced by cross-linking of TCR/MHC-peptide-CD8/p56lck adducts in rafts, Eur. J. Immunol. 31 (2001) 1561–1570.
[8] I.F. Luescher, E. Vivier, A. Layer, J. Mahiou, F. Godeau, B. Malissen, P. Romero, CD8 modulation of T-cell antigen receptor-ligand interactions on living cytotoxic T lymphocytes, Nature 373 (1995) 353–356.
[9] A.M. Moody, D. Chui, P.A. Reche, J.J. Priatel, J.D. Marth, E.L. Reinherz, Developmentally regulated glycosylation of the CD8alphabeta coreceptor stalk modulates ligand binding, Cell 107 (2001) 501–512.
[10] A.M. Moody, S.J. North, B. Reinhold, S.J. Van Dyken, M.E. Rogers, M. Panico, A. Dell, H.R. Morris, J.D. Marth, E.L. Reinherz, Sialic acid capping of CD8beta core 1-O-glycans controls thymocyte-major histocompatibility complex class I interaction, J. Biol. Chem. 278 (2003) 7240–7246.
[11] M.A. Daniels, L. Devine, J.D. Miller, J.M. Moser, A.E. Lukacher, J.D. Altman, P. Kavathas, K.A. Hogquist, S.C. Jameson, CD8 binding to MHC class I molecules is influenced by T cell maturation and glycosylation, Immunity 15 (2001) 1051–1061.
[12] L.G. Casabó, C. Mamalaki, D. Kioussis, R. Zamoyska, T cell activation results in physical modification of the mouse CD8 beta chain, J. Immunol. 152 (1994) 397–404.
[13] B.P. Pappu, P.A. Shrikant, Alteration of cell surface sialylation regulates antigen-induced naive CD8+ T cell responses, J. Immunol. 173 (2004) 275–284.
[14] L.E. Harrington, M. Galvan, L.G. Baum, J.D. Altman, R. Ahmed, Differentiating between memory and effector CD8 T cells by altered expression of cell surface O-glycans, J. Exp. Med. 191 (2000) 1241–1246.
[15] A.H. Merry, R.J. Gilbert, D.A. Shore, L. Royle, O. Miroshnychenko, M. Vuong, M.R. Wormald, D.J. Harvey, R.A. Dwek, B.J. Classon, P.M. Rudd, S.J. Davis, O-glycan sialylation and the structure of the stalk-like region of the T cell co-receptor CD8, J. Biol. Chem. 278 (2003) 27119–27228.
[16] J.P. Boursier, A. Alcover, F. Herve, I. Laisney, O. Acuto, Evidence for an extended structure of the T-cell co-receptor CD8 alpha as deduced from the hydrodynamic properties of soluble forms of the extracellular region, J. Biol. Chem. 268 (1993) 2013–2020.
[17] R. Wang, K. Natarajan, D.H. Margulies, Structural basis of the CD8 alpha beta/MHC class I interaction: focused recognition orients CD8 beta to a T cell proximal position, J. Immunol. 183 (2009) 2554–2564.
[18] S. Hennecke, P. Cosson, Role of transmembrane domains in assembly and intracellular transport of the CD8 molecule, J. Biol. Chem. 268 (1993) 26607–26612.
[19] P.S. Kern, M.K. Teng, A. Smolyar, J.H. Liu, J. Liu, R.E. Hussey, R. Spoerl, H.C. Chang, E.L. Reinherz, J.H. Wang, Structural basis of CD8 coreceptor function revealed by crystallographic analysis of a murine CD8alphaalpha ectodomain fragment in complex with H-2Kb, Immunity 9 (1998) 519–530.
[20] H.C. Chang, K. Tan, J. Ouyang, E. Parisini, J.H. Liu, Y. Le, X. Wang, E.L. Reinherz, J.H. Wang, Structural and mutational analyses of a CD8alphabeta heterodimer and comparison with the CD8alphaalpha homodimer, Immunity 23 (2005) 661–671.
[21] H.C. Chang, K. Tan, Y.M. Hsu, CD8alphabeta has two distinct binding modes of interaction with peptide-major histocompatibility complex class I, J. Biol. Chem. 281 (2006) 28090–28096.
[22] L. Devine, J. Sun, M.R. Barr, P.B. Kavathas, Orientation of the Ig domain of CD8β relative to MHC class I, J. Immunol. 162 (1999) 846–851.
[23] L. Devine, D. Thakral, S. Nag, J. Dobbins, M.E. Hodsdon, P.B. Kavathas, Mapping the binding site on CD8 beta for MHC class I reveals mutants with enhanced binding, J. Immunol. 177 (2006) 3930–3938.
[24] N. Auphan, C. Boyer, P. Andre, P. Bongrand, A.M. Schmitt-Verhulst, Biochemical and functional association between CD8 and H-2 at the surface of a T cell clone, Mol. Immunol. 28 (1991) 827–837.
[25] M.L. Blue, K.A. Craig, P. Anderson, K.R. Branton Jr., S.F. Schlossman, Evidence for specific association between class I major histocompatibility antigens and the CD8 molecules of human suppressor/cytotoxic cells, Cell 54 (1988) 413–421.
[26] J. Back, E.L. Malchiodi, S. Cho, L. Scarpellino, P. Schneider, M.C. Kerzic, R.A. Mariuzza, W. Held, Distinct conformations of Ly49 natural killer cell receptors mediate MHC class I recognition in trans and cis, Immunity 31 (2009) 598–608.
[27] J. Back, G.S. Angelov, R.A. Mariuzza, W. Held, The interaction with H-2D(d) in cis is associated with a conformational change in the Ly49A NK cell receptor, Front. Immunol. 2 (2011) 55, https://doi.org/10.3389/fimmu.2011.00055.
[28] Y. Li, R.A. Mariuzza, Structural basis for recognition of cellular and viral ligands by NK cell receptors, Front. Immunol. 5 (2014) 123, https://doi.org/10.3389/fimmu.2014.00123.
[29] Y. Bushkin, S. Demaria, J.M. Le, R. Schwab, Physical association between the CD8 and HLA class I molecules on the surface of activated human T lymphocytes, Proc. Natl. Acad. Sci. U.S.A. 85 (1988) 3985–3989.
[30] S.G. Santos, S.J. Powis, F.A. Arosa, Misfolding of major histocompatibility complex class I molecules in activated T cells allows cis-interactions with receptors and signaling molecules and is associated with tyrosine phosphorylation, J. Biol. Chem. 279 (2004) 53062–53070.
[31] S.J. de Vries, A.D. van Dijk, M. Krzeminski, M. van Dijk, A. Thureau, V. Hsu, T. Wassenaar, A.M. Bonvin, HADDOCK versus HADDOCK: new features and performance ofHADDOCK2.0 on the CAPRI targets, Proteins 69 (2007) 726–733.
[32] C. Dominguez, R. Boelens, A.M. Bonvin, HADDOCK: a protein-protein docking approach based on biochemical or biophysical information, J. Am. Chem. Soc. 125 (2003) 1731–1737.
[33] D.A. Shore, L. Teyton, R.A. Dwek, P.M. Rudd, I.A. Wilson, Crystal structure of the TCR co-receptor CD8alphaalpha in complex with monoclonal antibody YTS 105.18 Fab fragment at 2.88 A resolution, J. Mol. Biol. 358 (2006) 347–354.

[34] D.A. Shore, H. Issafras, E. Landais, L. Teyton, I.A. Wilson, The crystal structure of CD8 in complex with YTS156.7.7 Fab and interaction with other CD8 antibodies define the binding mode of CD8 alpha beta to MHC class I, J. Mol. Biol. 384 (2008) 1190–1202.
[35] L. Devine, M.E. Hodsdon, M.A. Daniels, S.C. Jameson, P.B. Kavathas, Location of the epitope for an anti-CD8alpha antibody 53.6.7 which enhances CD8alpha-MHC class I interaction indicates antibody stabilization of a higher affinity CD8 conformation, Immunol. Lett. 93 (2004) 123–130.
[36] T.K. Starr, M.A. Daniels, M.M. Lucido, S.C. Jameson, K.A. Hogquist, Thymocyte sensitivity and supramolecular activation cluster formation are developmentally regulated: a partial role for sialylation, J. Immunol. 171 (2003) 4512–4520.
[37] E. Jouanneau, K.L. Black, L. Veiga, R. Cordner, S. Goverdhana, Y. Zhai, X.X. Zhang, A. Panwar, A. Mardiros, H. Wang, A. Gragg, M. Zandian, D.K. Irvin, C.J. Wheeler, Intrinsically de-sialylated CD103(+) CD8 T cells mediate beneficial anti-glioma immune responses, Cancer Immunol. Immunother. 63 (2014) 911–924.
[38] M.J. Bijlmakers, Protein acylation and localization in T cell signaling, Mol. Membr. Biol. 26 (2009) 93–103.
[39] D. Filipp, O. Ballek, J. Manning, Lck, membrane microdomains, and TCR triggering machinery: defining the new rules of engagement, Front. Immunol. 3 (2012) 155.
[40] V. Horejsí, The roles of membrane microdomains (rafts) in T cell activation, Immunol. Rev. 191 (2003) 148–164.
[41] L. Rettig, L. McNeill, N. Sarner, P. Guillaume, I. Luescher, M. Tolaini, D. Kioussis, R. Zamoyska, An essential role for the stalk region of CD8 beta in the coreceptor function of CD8, J. Immunol. 182 (2009) 121–129.
[42] J.S. Wong, X. Wang, T. Witte, L. Nie, N. Carvou, P. Kern, H.C. Chang, Stalk region of beta-chain enhances the coreceptor function of CD8, J. Immunol. 171 (2003) 867–874.
[43] Y.J. Kang, X. Wang, S.J. Lin, Y.M. Hsu, H.C. Chang, An active CD8alpha/pMHCI interaction is required for CD8 single positive thymocyte differentiation, Eur. J. Immunol. 40 (2010) 836–848.
[44] J. Huang, L.J. Edwards, B.D. Evavold, C. Zhu, Kinetics of MHC-CD8 interaction at the T cell membrane, J. Immunol. 179 (2007) 7653–7662.
[45] Y. Narimatsu, T. Kubota, S. Furukawa, H. Morii, H. Narimatsu, K. Yamasaki, Effect of glycosylation on cis/trans isomerization of prolines in IgA1-hinge peptide, J. Am. Chem. Soc. 132 (2010) 5548–5549.
[46] J. Chen, S.A. Edwards, F. Gräter, C. Baldauf, On the cis to trans isomerization of prolyl-peptide bonds under tension, J. Phys. Chem. B 116 (2012) 9346–9351.
[47] G. Kovalev, K. Duus, L. Wang, R. Lee, M. Bonyhadi, D. Ho, J.M. McCune, H. Kaneshima, L. Su, Induction of MHC class I expression on immature thymocytes in HIV-1-infected SCID-hu Thy/Liv mice: evidence of indirect mechanisms, J. Immunol. 162 (1999) 7555–7562.
[48] G. Schönrich, G. Strauss, K.P. Müller, L. Dustin, D.Y. Loh, N. Auphan, A.M. Schmitt-Verhulst, B. Arnold, G.J. Hämmerling, Distinct requirements of positive and negative selection for selecting cell type and CD8 interaction, J. Immunol. 151 (1993) 4098–4105.
[49] C. Büll, T.J. Boltje, N. Balneger, S.M. Weischer, M. Wassink, J.J. van Gemst, V.R.L.J. Bloemendal, L. Boon, J. van der Vlag, T. Heise, M.H. den Brok, G.J. Adema, Sialic acid blockade suppresses tumor growth by enhancing T cell-mediated tumor immunity, Cancer Res. 78 (2018) 3574–3588.
[50] D.A. Lawrence, R. Song, P. Weber, Surface thiols of human lymphocytes and their changes after in vitro and in vivo activation, J. Leukoc. Biol. 60 (1996) 611–618.
[51] P. Castellani, G. Angelini, L. Delfino, A. Matucci, A. Rubartelli, The thiol redox state of lymphoid organs is modified by immunization: role of different immune cell populations, Eur. J. Immunol. 38 (2008) 2419–2425.
[52] P. Kesarwani, A.A. Al-Khami, G. Scurti, K. Thyagarajan, N. Kaur, S. Husain, Q. Fang, O.S. Naga, P. Simms, G. Beeson, C. Voelkel-Johnson, E. Garrett-Mayer, C.C. Beeson, M.I. Nishimura, S. Mehrotra, Promoting thiol expression increases the durability of antitumor T-cell functions, Cancer Res. 74 (2014) 6036–6047.
[53] M.A. Daniels, K.A. Hogquist, S.C. Jameson, Sweet 'n' sour: the impact of differential glycosylation on T cell responses, Nat. Immunol. 3 (2002) 903–910.
[54] Q.R. Johnson, R.J. Lindsay, S.R. Raval, J.S. Dobbs, R.B. Nellas, T. Shen, Effects of branched O-glycosylation on a semiflexible peptide linker, J. Phys. Chem. B 118 (2014) 2050–2057.
[55] J.J. Priatel, D. Chui, N. Hiraoka, C.J. Simmons, K.B. Richardson, D.M. Page, M. Fukuda, N.M. Varki, J.D. Marth, The ST3Gal-I sialyltransferase controls CD8+ T lymphocyte homeostasis by modulating O-glycan biosynthesis, Immunity 12 (2000) 273–283.
[56] W. Held, R.A. Mariuzza, Cis-trans interactions of cell surface receptors: biological roles and structural basis, Cell. Mol. Life Sci. 68 (2011) 3469–3478.
[57] M.L. Deftos, Y.W. He, E.W. Ojala, M.J. Bevan, Correlating notch signaling with thymocyte maturation, Immunity 9 (1998) 777–786.
[58] C. Cepko, W. Pear, Retrovirus infection of cells in vitro and in vivo, Curr Protoc Mol Biol. (2001), https://doi.org/10.1002/0471142727.mb0914s36. Chapter 9: Unit 9.14, John Wiley & Sons online library.
[59] S.P. Kerkar, L. Sanchez-Perez, S. Yang, Z.A. Borman, P. Muranski, Y. Ji, D. Chinnasamy, A.D. Kaiser, C.S. Hinrichs, C.A. Klebanoff, C.D. Scott, L. Gattinoni, R.A. Morgan, S.A. Rosenberg, N.P. Restifo, Genetic engineering of murine CD8+ and CD4+ T cells for preclinical adoptive immunotherapy studies, J. Immunother. 34 (2011) 343–352.
[60] J. Leignadier, S. Favre, S.A. Luther, I.F. Luescher, CD8 engineered cytotoxic T cells reprogram melanoma tumor environment, Oncoimmunology 5 (2015), e1086861, https://doi.org/10.1080/2162402X.2015.1086861.
[61] L.M. Loura, M. Prieto, FRET in membrane biophysics: an overview, Front. Physiol. 2 (2011) 82, https://doi.org/10.3389/fphys.2011.00082.
[62] M.A. Digman, V.R. Caiolfa, M. Zamai, E. Gratton, The phasor approach to fluorescence lifetime imaging analysis, Biophys. J. 94 (2008) L14–L16.
[63] E.F. Pettersen, T.D. Goddard, C.C. Huang, G.S. Couch, D.M. Greenblatt, E.C. Meng, T.E. Ferrin, UCSF Chimera–a visualization system for exploratory research and analysis, J. Comput. Chem. 25 (2004) 1605–1612.
[64] M. Durairaj, R. Sharma, J.C. Varghese, K.P. Kane, Requirement for Q226, but not multiple charged residues, in the class I MHC CD loop/D strand for TCR-activated CD8 accessory function, Eur. J. Immunol. 33 (2003) 676–684.

[65] M. Sekimata, M. Tanabe, A. Sarai, J. Yamamoto, A. Kariyone, H. Nakauchi, K. Egawa, M. Takiguchi, Different effects of substitutions at residues 224 and 228 of MHC class I on the recognition of CD8, J. Immunol. 150 (1993) 4416–4426.

[66] J.M. Connolly, T.H. Hansen, A.L. Ingold, T.A. Potter, Recognition by CD8 on cytotoxic T lymphocytes is ablated by several substitutions in the class I alpha 3 domain: CD8 and the T-cell receptor recognize the same class I molecule, Proc. Natl. Acad. Sci. U.S.A. 87 (1990) 2137–2141.